iScience

CellPress
OPEN ACCESS

Article

Diverse effector and regulatory functions of fibro/adipogenic progenitors during skeletal muscle fibrosis in muscular dystrophy

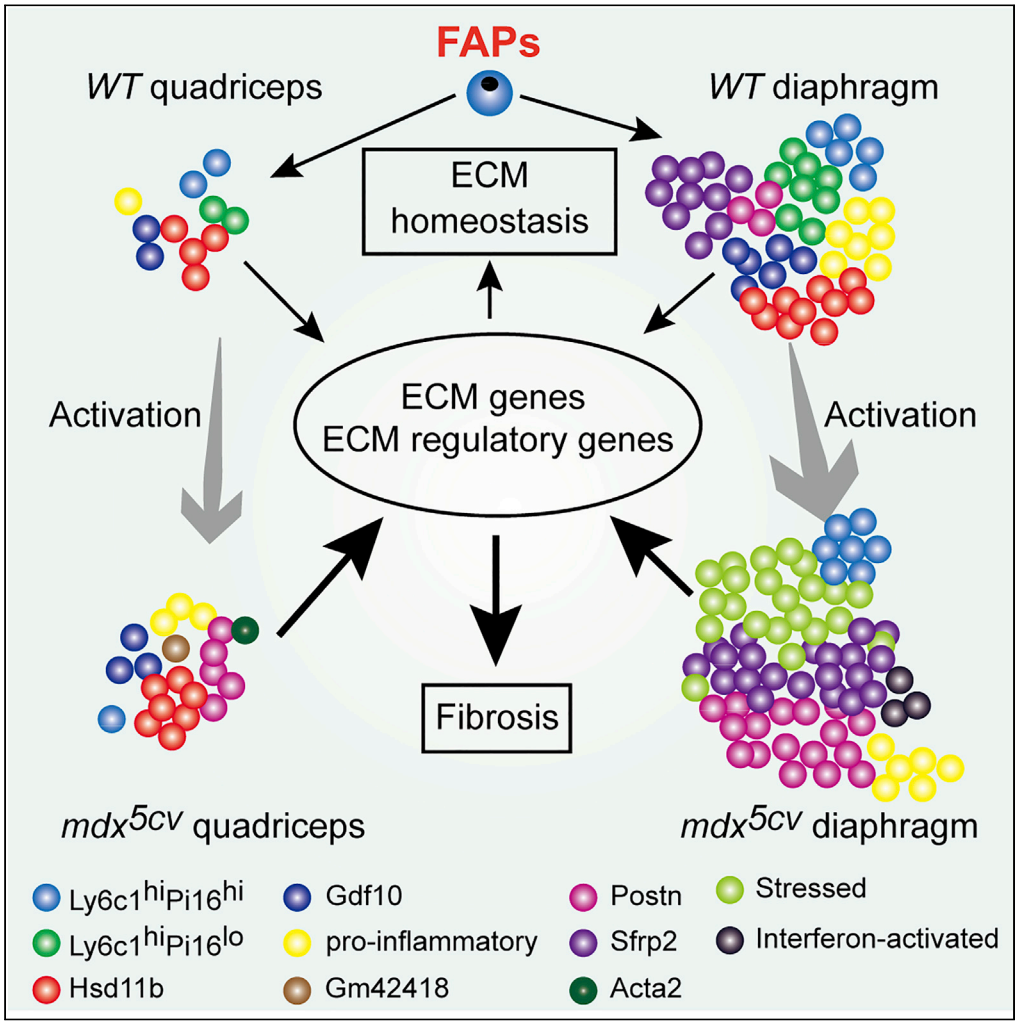

Xingyu Wang, Jianming Chen, Sachiko T. Homma, ..., Frederique Ruf-Zamojski, Stuart C. Sealfon, Lan Zhou

lanzhou@bu.edu

Highlights

scRNAseq supports the effector and regulatory functions of FAPs in muscle fibrosis

FAPs are more abundant in the diaphragm than in quadriceps

Diaphragm and quadriceps FAPs contain different clusters in the steady state

Diaphragm and quadriceps FAPs respond differently to muscular dystrophy

Wang et al., iScience 26, 105775
January 20, 2023
https://doi.org/10.1016/j.isci.2022.105775

iScience

CellPress
OPEN ACCESS

Article

Diverse effector and regulatory functions of fibro/adipogenic progenitors during skeletal muscle fibrosis in muscular dystrophy

Xingyu Wang,[1,3,4] Jianming Chen,[1,3] Sachiko T. Homma,[1] Yinhang Wang,[1] Gregory R. Smith,[2] Frederique Ruf-Zamojski,[2] Stuart C. Sealfon,[2] and Lan Zhou[1,*]

SUMMARY

Fibrosis is a prominent pathological feature of skeletal muscle in Duchenne muscular dystrophy (DMD). The commonly used disease mouse model, *mdx*^{5cv}, displays progressive fibrosis in the diaphragm but not limb muscles. We use single-cell RNA sequencing to determine the cellular expression of the genes involved in extracellular matrix (ECM) production and degradation in the *mdx*^{5cv} diaphragm and quadriceps. We find that fibro/adipogenic progenitors (FAPs) are not only the primary source of ECM but also the predominant cells that express important ECM regulatory genes, including *Ccn2*, *Ltbp4*, *Mmp2*, *Mmp14*, *Timp1*, *Timp2*, and *Loxs*. The effector and regulatory functions are exerted by diverse FAP clusters which are different between diaphragm and quadriceps, indicating their activation by different tissue microenvironments. FAPs are more abundant in diaphragm than in quadriceps. Our findings suggest that the development of anti-fibrotic therapy for DMD should target not only the ECM production but also the pro-fibrogenic regulatory functions of FAPs.

INTRODUCTION

Duchene muscular dystrophy (DMD) is the most common genetic muscle disease, which is lethal with no cure currently.[1,2] It is an X-linked recessive disease caused by the defective dystrophin gene. Fibrosis is a prominent pathologic feature of skeletal muscle, which directly contributes to muscle weakness.[3,4] Development of effective anti-fibrotic therapies relies on the understanding of molecular and cellular mechanisms mediating and regulating muscle fibrosis. The commonly used DMD mouse models, *mdx* and *mdx*^{5cv}, show progressive fibrosis in the diaphragm but not limb muscles.[5–8] Little is known why limb and respiratory muscles show such a difference, and understanding the cellular and molecular contributions to the difference may benefit the anti-fibrotic therapy development.

Fibrosis is characterized by excessive accumulation of extracellular matrix (ECM) proteins that consist of collagens, fibronectin, and proteoglycans.[9–11] Fibrosis development and progression in skeletal muscle can be promoted at different levels, including ECM gene upregulation stimulated by pro-fibrogenic factors such as transforming growth factor β1 (TGF-β1),[12] connective tissue growth factor (CTGF),[13] and osteopontin,[14–16] reduced matrix metalloproteinases (MMPs)-mediated ECM protein degradation,[17] increased tissue inhibitors of matrix metalloproteinases (TIMPs),[17] and heightened collagen cross-linking catalyzed by lysyl oxidases (LOXs), which makes ECM stiff and resistant to proteolytic degradation.[18,19]

Fibro/adipogenic progenitors (FAPs) are muscle interstitial mesenchymal progenitors, expressing mesodermal marker PDGFRα and stem cell markers Sca-1 and CD34. They are bipotent progenitors that can differentiate into fibroblasts and adipocytes.[20–22] They play important roles in skeletal muscle injury and repair.[22,23] Upon injury, they become activated, proliferating and expanding rapidly.[20,24,25] They provide a favorable tissue environment to promote satellite cell-mediated muscle regeneration.[20,26–29] As muscle regeneration proceeds, excessive FAPs are cleared from the regenerative niche by apoptosis.[25] Failing to do so leads to the pathological accumulation of FAPs, contributing to fibro-fatty replacement of muscle.[21,25]

In the present study, we performed single-cell RNA sequencing (scRNAseq) to determine the cellular expression of the genes involved in ECM production and degradation during skeletal muscle fibrosis in

[1]Department of Neurology, Boston University School of Medicine, 72 East Concord Street, Boston, MA 02118, USA

[2]Department of Neurology, Icahn School of Medicine at Mount Sinai, 1468 Madison Avenue, New York, NY 10029, USA

[3]These authors contributed equally

[4]Lead contact

*Correspondence: lanzhou@bu.edu

https://doi.org/10.1016/j.isci.2022.105775

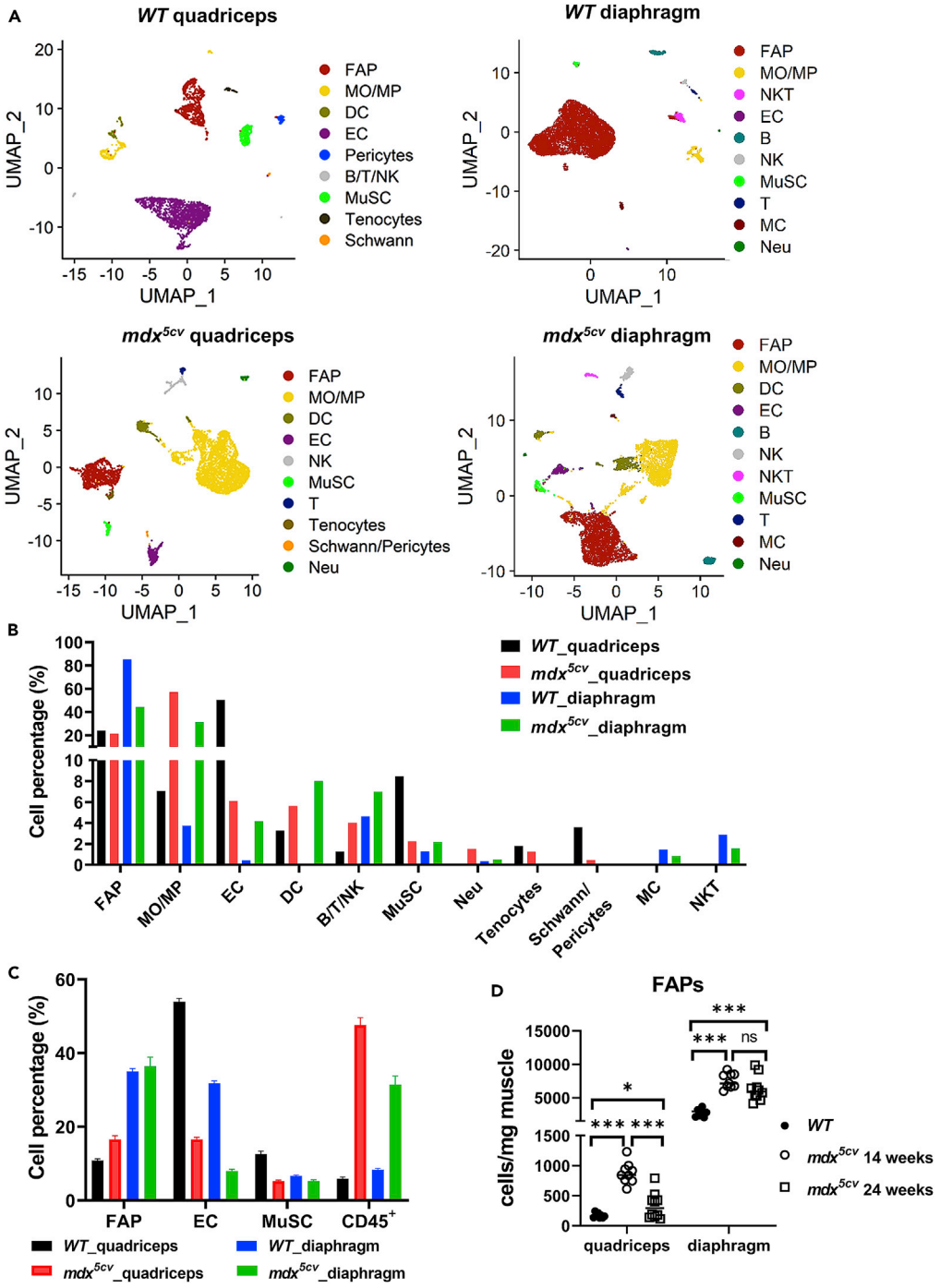

Figure 1. FAPs are the most abundant among mononuclear cells in diaphragm but not quadriceps of both wild-type (*WT*) and *mdx*^{5cv} mice

(A) Uniform Mani-fold Approximation and Projection (UMAP) dimension reduction analysis showing different cell types in *WT* and *mdx*^{5cv} quadriceps and diaphragm muscles. FAP: Fibro/adipogenic progenitors, MO/MP: Monocyte/Macrophages, DC: Dendritic cells, EC: Endothelial cells, MuSC: Myogenic stem cells, B: B cells, T: T cells, NK: Natural killer cells, NKT: invariant Natural Killer T Cells, MC: Mesothelial cells, Neu: Neutrophils.

(B) Bar graph showing percentage of each cell type to total cells analyzed by scRNAseq in each indicated muscle sample, quantified by UMAP analysis.

(C) Bar graph showing percentages of FAP, EC, MuSC, and CD45^{+} cells to total mononuclear cells, quantified by FACS, in each indicated muscle sample (Qua.: quadriceps; Dia.: diaphragm).

Figure 1. *Continued*
(D) Scatterplot showing and comparing cell densities of FAPs in *WT* quadriceps, *WT* diaphragm, *mdx*^{5cv} quadriceps, and *mdx*^{5cv} diaphragm determined by FACS analysis. Data are represented as mean ± SEM Asterisks indicate significant differences (*p < 0.05, ***p < 0.001, ns: no significance, Kruskal-Wallis test followed by Dunn's test for multiple comparisons).

mdx^{5cv}, and to identify differences between diaphragm and quadriceps. Our findings demonstrate that FAPs are not only the key effector cells that express a high level of ECM genes, but also the predominant regulatory cells that express a high level of *Ccn2*, *Ltbp4*, *Mmp2, Mmp14*, *Timp1, Timp2*, and *Loxs* to regulate ECM production and degradation. The effector and regulatory functions are exerted by diverse FAP clusters, which are different between diaphragm and quadriceps, indicating different tissue microenvironments in these two types of skeletal muscles. FAPs are much more abundant in diaphragm than in quadriceps. FAPs are the key effectors and regulators of *mdx*^{5cv} diaphragm fibrosis.

RESULTS

Fibro/adipogenic progenitors are the most abundant mononuclear cells in diaphragm but not quadriceps of both wild-type and *mdx*^{5cv} mice

Muscle necrosis, inflammation, and fibrosis are evident in both diaphragm and quadriceps muscles of *mdx*^{5cv} at 14 weeks of age. However, these changes subside afterward in the quadriceps with progressive fibrosis mainly seen in the diaphragm at 24 weeks of age (Figure S1A).[5,30] To uncover the cellular and molecular differences accounting for the divergent fibrosis progression, we performed scRNAseq using single-cell suspensions prepared from diaphragm and quadriceps of *mdx*^{5cv} and *WT* mice at 14 weeks of age. The single-cell suspensions contain mononuclear cells but not myofibers, as polynuclear myofibers cannot be included due to their large size. scRNAseq of the four muscle samples, each pooled from five male mice, were performed simultaneously (see Table S1 for quality control). By filtering out the cells of low quality,[31] we obtained 16,766 genes from 3,814 cells of *WT* quadriceps, 17,677 genes from 6,988 cells of *WT* diaphragm, 18,398 genes from 6,302 cells of *mdx*^{5cv} quadriceps, and 18,152 genes from 6,089 cells of *mdx*^{5cv} diaphragm for analysis. Sequencing data were first analyzed using Uniform Mani-fold Approximation and Projection (UMAP) for dimension reduction to generate functionally enriched clusters in each sample. The identities of the generated clusters were determined by the expression of cell type-specific marker genes (Figure S2). Multiple cell types were identified in each sample (Figures 1A and S2, Tables S2 and S3). Most of the cell types were present in all four samples, but mesothelial cells (MCs) and invariant natural killer T cells (NKT) cells were only identified in diaphragm, while Schwann cells, pericytes, and tenocytes were only identified in quadriceps (Figure 1A). Mesothelium covers the surface of diaphragm but not quadriceps,[32] which explains the detection of MCs only in diaphragm. The lack of other cell types in diaphragm or quadriceps is likely due to their very low abundance. Clusters with a high-level expression of *Pdgfra*, *Ly6a*, and *Cd34* and lack of expression of *Pecam1*, *Ptprc*, *Itga7*, *Tnmd*, and *Fmod* were identified as FAPs (Figure S2B).

In both *WT* and *mdx*^{5cv} diaphragm, FAPs were the most abundant cell type identified by scRNAseq (Figure 1A). Endothelial cells (ECs) and monocytes/macrophages (MOs/MPs) were the most abundant cell types in *WT* and *mdx*^{5cv} quadriceps, respectively (Figures 1A and 1B and Table S3). Since the cell representation could be altered by multiple processing steps of scRNAseq, we further determined the relative abundance of FAPs, ECs, myogenic stem cells (MuSCs), and CD45^{+} cells (contain MOs/MPs) by flow cytometry analysis (FACS) (Figures 1C and S1B). FACS and scRNAseq revealed similar percentages of these cells, except for the ECs in *WT* diaphragm, which showed a much lower percentage by scRNAseq than by FACS (Figures 1B and 1C). FAPs are therefore over-represented in *WT* diaphragm by scRNAseq. But FACS also showed that FAP was the most abundant cell type in *WT* diaphragm (Figure 1C). The FAP cell density, determined by FACS, was markedly higher in diaphragm than in quadriceps (Figure 1D). It increased dramatically in both quadriceps and diaphragm of *mdx*^{5cv} as compared with *WT* at 14 weeks of age, but it was then reduced in *mdx*^{5cv} quadriceps while remained high in *mdx*^{5cv} diaphragm at 24 weeks of age (Figure 1D), corresponding to the progressive fibrosis seen in *mdx*^{5cv} diaphragm but not quadriceps (Figure S1). The findings are consistent with previous studies reporting a higher level of PDGFRα protein expression in diaphragm than in limb muscles.[33–35]

Fibro/adipogenic progenitors are the primary cells expressing extracellular matrix genes in the skeletal muscle of both wild-type and *mdx*^{5cv} mice

FAPs are known ECM-producing cells.[36] To determine the relative contribution of different cell types to ECM production, we compared the cellular expression of the genes encoding collagens, fibronectin,

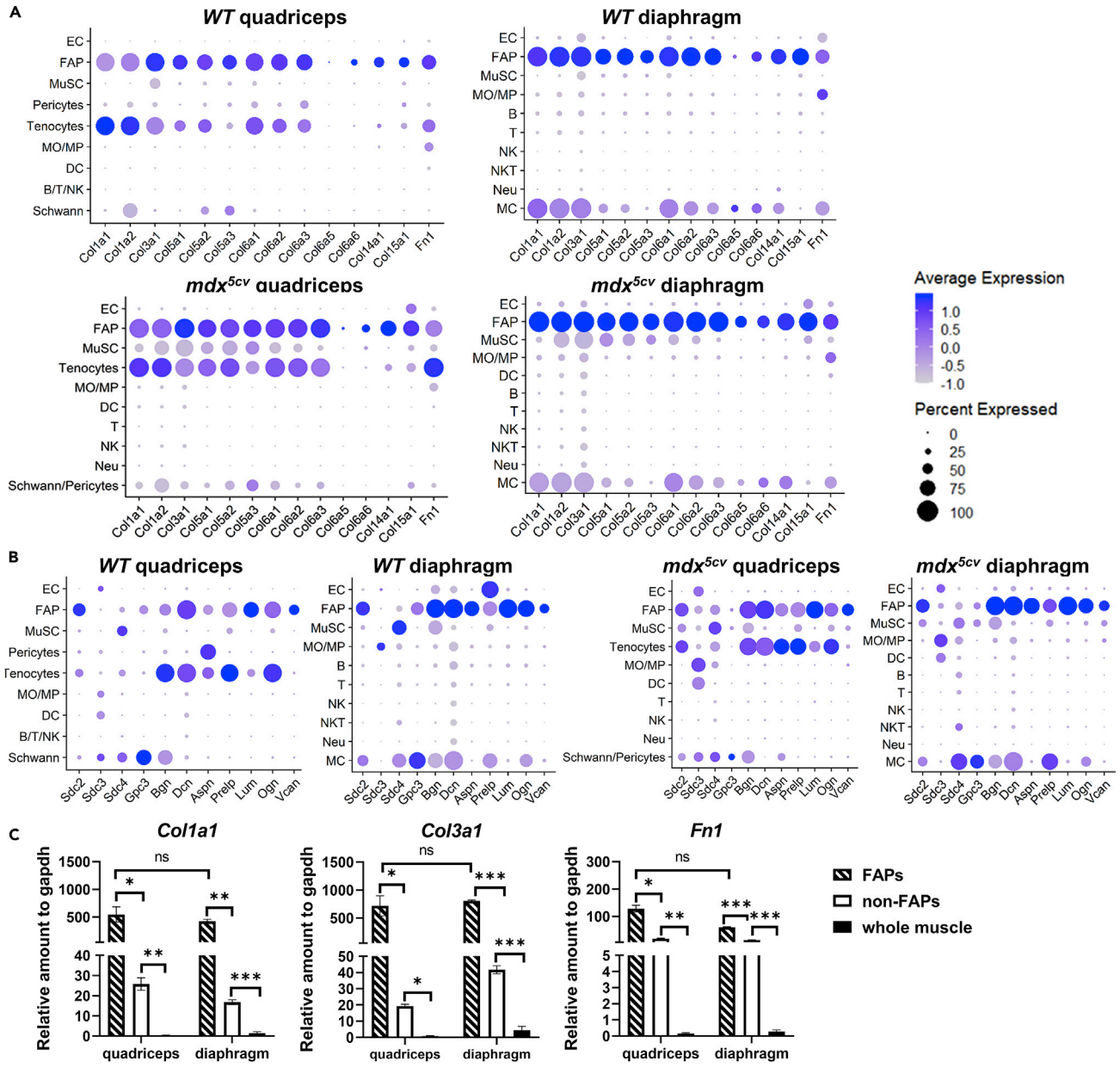

Figure 2. FAPs are the predominant cells expressing extracellular matrix (ECM) genes in both *WT* and *mdx*^{5cv} quadriceps and diaphragm

(A) Dot plot showing the expression of collagen and fibronectin genes by different cell types in different muscles. The dot color intensity reflects the average gene expression level, and the dot size represents the percentage of the cells expressing the gene.

(B) Dot plot showing the expression of proteoglycan genes.

(C) qRT-PCR showing and comparing *Col1a1* and *Col3a1*, and *Fn1* expression by FACS-sorted FAPs, FACS-sorted non-FAPs, and whole muscle of *mdx*^{5cv} quadriceps and diaphragm at 14 weeks of age. Data are represented as mean ± SEM Asterisks indicate significant differences (*p < 0.05, **p < 0.01, ***p < 0.001, ns: no significance, Kruskal-Wallis test followed by Dunn's test for multiple comparisons). N = 5 mice/group.

proteoglycans, and synthesizing enzymes for glycosaminoglycans (GAGs) which are the components of many proteoglycans[10] (Figures 2, S3, and S4). For all the collagen genes with detectable expression by scRNAseq, the high expression was predominantly detected in FAPs, as well as tenocytes in quadriceps, which include *Col1s* and *Col3s* that encode collagen I and collagen III, the two major fibrillary collagen constituents in interstitial tissue of skeletal muscle[37] (Figures 2A and S3). FAPs and quadriceps tenocytes were also the major cell types that expressed a high level of fibronectin gene (*Fn1*) (Figure 2A) and many

proteoglycan genes (Figures 2B and S4A). In addition, FAPs moderately expressed several genes encoding the synthesizing enzymes of GAGs (Figure S4B). MCs, Schwann cells, pericytes, and MuSCs also expressed multiple ECM genes but at a lower level (Figures 2A and 2B). Considering the relative low abundance, their contribution to the ECM production is likely limited. To determine the potential contribution by myofibers which cannot be included for scRNAseq, we performed quantitative reverse-transcription PCR (qRT-PCR) to compare FACS-sorted FAPs, FACS-sorted non-FAP cells, and whole muscle tissue samples from *mdx*^{5cv} mice. The mRNA expression of *Col1a1*, *Col3a1*, and *Fn1* by the whole muscle tissue was significantly lower than that by the two sorted cell samples (Figure 2C), indicating that myofibers do not significantly contribute to ECM production in dystrophic muscles. Together, our findings are consistent with the notion that FAPs are the key ECM-producing cells in skeletal muscle in both steady state and *mdx*^{5cv}. Given the persistent high FAP density in *mdx*^{5cv} diaphragm (Figure 1C), FAPs are the main effector cells mediating the progression of fibrosis in this muscle.

Fibro/adipogenic progenitors are the predominant cells expressing many regulatory genes involved in skeletal muscle extracellular matrix production and degradation

To address which cell types are the key regulators of skeletal muscle fibrosis, we next analyzed the cellular expression of the genes encoding fibrogenic factors, MMPs, TIMPs, and LOXs.

Among the genes that regulate FAP activation and ECM production (Figures 3A and S5A), the CTGF gene (*Ccn2*), insulin-like growth factor-1 (IGF-1) gene (*Igf1*), and follistatin gene (*Fst*) were preferentially expressed by FAPs in both *WT* and *mdx*^{5cv} diaphragm. In quadriceps, tenocytes expressed a higher level of *Ccn2* and *Igf1* than FAPs, while FAPs were the major source of *Fst*. FAPs also expressed a high level of latent TGFβ binding protein 4 gene (*Ltbp4*). The FAP expression of these genes has also been reported by other studies.[20,24,27,38,39] The findings indicate that FAPs regulate their own differentiation and ECM gene expression. FAPs in diaphragm and tenocytes in quadriceps expressed a high level of *Tgfb3*. *Tgfb1* and *Spp1*, the two potent pro-fibrogenic genes, were mostly expressed by MOs/MPs in *mdx*^{5cv}, consistent with the notion that MOs/MPs promote muscle fibrosis in *mdx*.[40,41] MuSCs were the predominant cells expressing *Tgfb2* and *Pdgfa* in *mdx*^{5cv} but not *WT* muscles, indicating their acquired fibrogenic potential in *mdx*^{5cv}. *Pdgfb* was mainly expressed by ECs in *mdx*^{5cv} muscles. These findings are consistent with the previous report.[42] IFN-γ gene (*Ifng*) was mostly expressed by NK cells. Taken together, different fibrogenic factor genes are preferentially expressed by different cells, with FAPs, tenocytes, and immune cells being the most important contributors. The contribution of MCs to diaphragm fibrosis is likely limited due to their rarity.

Fibrosis is regulated not only at the level of ECM production but also at the level of ECM degradation. We next addressed which cells expressed *Mmps*, *Timps*, and *Loxs* to regulate ECM degradation (Figures 3B, 3C, and S5B). Among all the *Mmps*, *Mmp2*, *Mmp9*, and *Mmp14* were strongly expressed (Figure S5B), with the expression of *Mmp2* and *Mmp14* mainly by FAPs and tenocytes while the expression of *Mmp9* by neutrophils (Figure 3B). *Timps* were expressed by multiple cell types (Figure 3B), but *Timp1* and *Timp2* were preferentially expressed by FAPs and tenocytes. ECs were the main cells expressing *Timp3* and *Timp4*, except for *WT* diaphragm where the *Timp4* expression was diminished. Therefore, FAPs appear to play an active role in regulating ECM degradation. The genes that encode cross-linking enzymes, LOXs, were mainly expressed by FAPs and tenocytes (Figure 3C). FAPs may thus also regulate collagen cross-linking.

Taken together, FAPs actively express *Ccn2*, *Ltbp4*, *Igf1*, *Fst*, *Mmp2*, *Mmp14*, *Timp1*, *Timp2*, and *Lox* genes in skeletal muscle, regulating ECM production and degradation. Quantitative RT-PCR with FACS-sorted FAPs and non-FAP cells, as well as whole muscle samples, confirmed the major contribution of FAPs to the ECM regulatory gene expression in *mdx*^{5cv} quadriceps and diaphragm (Figure 3D). The findings support the notion that FAPs may play a key role not only in mediating but also in regulating skeletal muscle ECM homeostasis in the steady state and fibrosis in muscular dystrophy.[21,24,25,33,35,43–45]

Fibro/adipogenic progenitors in *mdx*^{5cv} diaphragm and quadriceps display differences in transcriptomes

Since FAPs not only produce ECM but also regulate ECM production and degradation, we next determined whether the transcriptomes of FAPs in *mdx*^{5cv} quadriceps and diaphragm are different to account for the divergent fibrosis progression in these two muscles. To this end, transcriptome data of FAPs

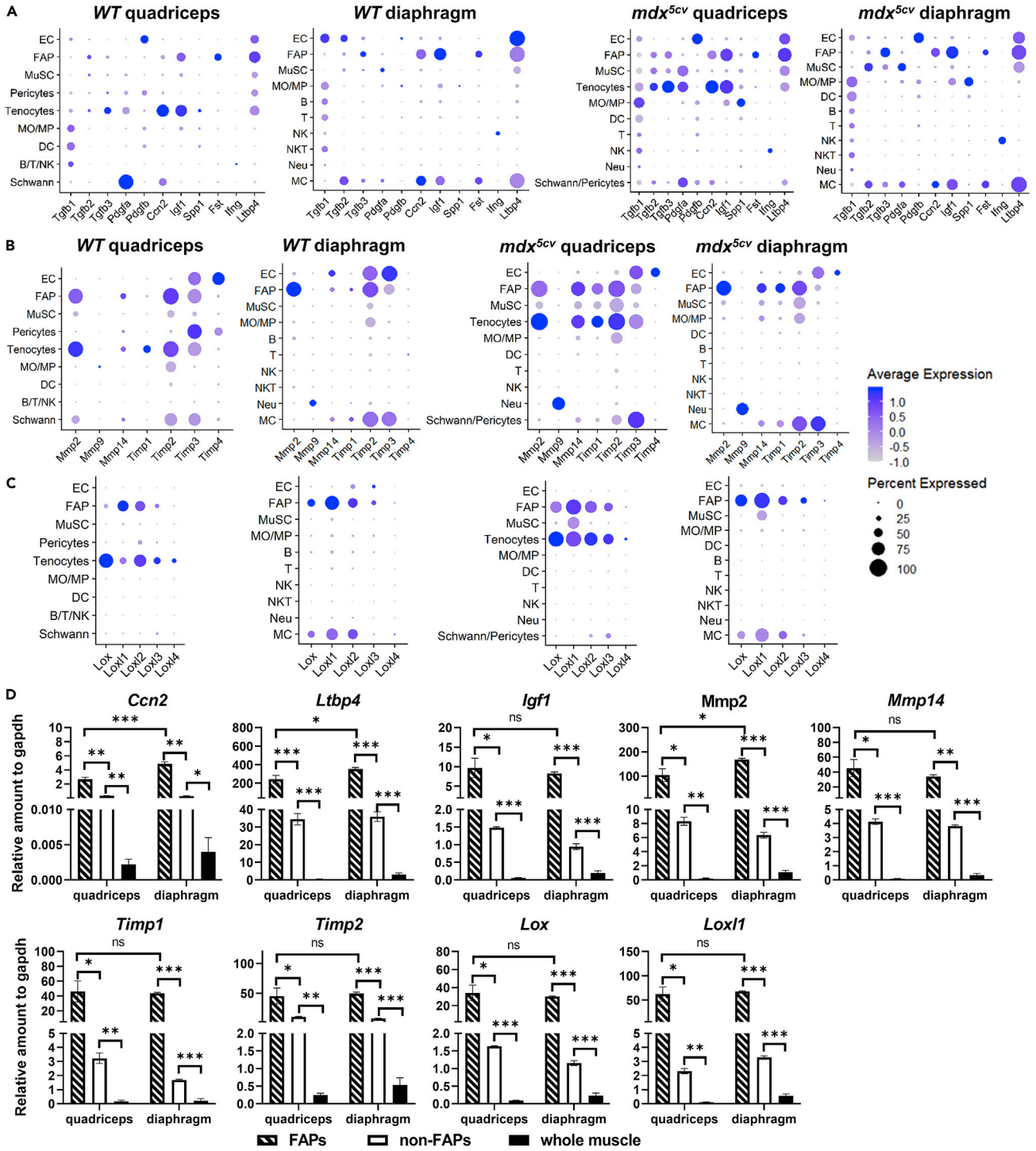

Figure 3. FAPs are the predominant cells expressing important regulatory genes of ECM production and degradation

(A-C) Dot plots showing the expression of fibrogenic factor genes (A), *Mmps* (B), *Timps* (B), and *Loxs* (C) by different cell types in quadriceps and diaphragm of *WT* and *mdx*^{5cv} mice.

(D) qRT-PCR showing and comparing the expression of selected ECM regulatory genes by FACS-sorted FAPs, FACS-sorted non-FAPs, and whole muscle of *mdx*^{5cv} quadriceps and diaphragm at 14 weeks of age. Data are represented as mean ± SEM Asterisks indicate significant differences (*p < 0.05; **p < 0.01; ***p < 0.001; ns: no significance, Kruskal-Wallis test followed by Dunn's test for multiple comparisons). N = 5 mice/group.

from all four muscle samples (*WT* quadriceps: 846 cells; *WT* diaphragm: 5,829 cells; *mdx*^{5cv} quadriceps: 1,140 cell; *mdx*^{5cv} diaphragm: 2,515 cells) were merged and analyzed for differentially expressed genes (DEGs, $\log_2$FC $\geq$ 0.5 compared to the average expression level). UMAP analysis showed that FAP transcriptomes were different by the muscle type (quadriceps vs. diaphragm) and the disease state (*WT* vs. *mdx*^{5cv}) (Figure 4A), with 835 distinct DEGs identified in *mdx*^{5cv} quadriceps and 78 in *mdx*^{5cv} diaphragm (Figure 4B and Data S1). The DEGs in *mdx*^{5cv} quadriceps FAPs were functionally enriched in signaling pathways of TNF-α, IL-4 and IL-13, TGF-β, PDGF, and HGF, and in biological processes of cell migration, apoptosis, and angiogenesis. The DEGs in *mdx*^{5cv} diaphragm FAPs were functionally enriched in TGF-β response and ECM regulation. It is surprising that most of the ECM genes, fibrogenic factor genes, *Mmps*, *Timps*, and *Loxs* were not present in the distinct DEGs of *mdx*^{5cv} quadriceps or diaphragm FAPs (Data S1). Likewise, qRT-PCR showed no significant difference in *Col1a1*, *Col3a1*, *Fn*, *Igf1*, *Mmp14*, *Timp1*, *Timp2*, *Lox*, and *Loxl1* expression between *mdx*^{5cv} quadriceps and diaphragm FAPs (Figures 2C and 3D). The expression of *Ccn2*, *Ltbp4*, and *Mmp2* only showed a less than 2-fold increase in *mdx*^{5cv} diaphragm FAPs as compared with *mdx*^{5cv} quadriceps FAPs (Figure 3D). Therefore, there is no significant difference in the FAP expression of the ECM or ECM regulatory genes at a single-cell level between the two muscles. However, the gene expression of *Col1a1*, *Col3a1*, *Igf1*, *Mmp2*, *Mmp14*, *Lox* and *Loxl1* (Figure 4C) and the protein expression of collagen I, collagen III, and fibronectin (Figures 4D and S3B) at a whole-muscle level was significantly higher in *mdx*^{5cv} diaphragm than in *mdx*^{5cv} quadriceps, which is most likely contributed by the higher FAP density in *mdx*^{5cv} diaphragm.

Fibro/adipogenic progenitors consist of diverse clusters which are different between quadriceps and diaphragm in wild-type and *mdx*^{5cv} mice

FAPs are functionally heterogeneous in both steady state and disease state.[22,36,44,46–49] There are three types of tissue fibroblast clusters: universal clusters that are shared by all tissue fibroblasts in the steady state, specialized clusters that are induced by the tissue-specific microenvironment in the steady state, and activated clusters that are induced by a disease.[50] We next addressed whether quadriceps and diaphragm have different specialized FAP clusters in the steady state and different activated FAP clusters in *mdx*^{5cv} and whether different FAP clusters exert different effector and regulatory functions. To this end, we extracted transcriptome data of FAPs and re-clustered by UMAP analysis. Multiple clusters with differential transcriptomes were identified in each sample (Figures 5A and S6A).

Five FAP clusters were identified in *WT* quadriceps. The two universal clusters identified by the cross-tissue transcriptome analysis of fibroblasts,[50] including the adventitial stromal cell-like fibroblasts featured by *Ly6c1*, *Pi16*, *Dpp4*, and *CD55* and the basement membrane-associated fibroblasts featured by *Hsd11b1*, *Cxcl14*, *Col4a1*, *Col15a1*, and *Hspg2*,[50] were identified in our *WT* quadriceps FAPs and named Ly6c1^{hi} and Hsd11b1 clusters, respectively (Figures 5A, 6A-6C, and S6A.1; Table S4). Similar FAP clusters were also identified by two previous transcriptome studies[36,46] and named Dpp4^{+} and Cxcl14^{+} clusters.[46] The findings confirm the reliability of our analysis. We named the clusters with different featured genes to best distinguish them from the other clusters in all four samples. Interestingly, we identified two adventitial Ly6c1^{hi} FAP clusters, which were distinguished by the expression level of *Pi16*: Ly6c1^{hi}Pi16^{hi} and Ly6c1^{hi} Pi16^{lo} (Figures 5A and 6B; Table S4). Compared to the Ly6c1^{hi}Pi16^{hi} cluster, the Ly6c1^{hi}Pi16^{lo} cluster expressed a lower level of *Dpp4* but a higher level of *Col4a1* (Figures 6B and 6C), suggesting that this is an intermediate cluster between the adventitia stromal cell-like and basement membrane-associated clusters. The Ly6c1^{hi} clusters expressed the highest level of mesenchymal progenitor markers *Cd34* and *Ly6a/Sca-1* (Figure 6A), indicating their higher stemness than the other clusters. Pseudotime analysis confirmed the progenitor status of the Ly6c1^{hi}Pi16^{hi} cluster (Figure 5B), consistent with the finding by others.[50] The Ly6c1^{hi} clusters also expressed the highest level of TEK tyrosine kinase gene (*Tek*) (Figure 6B), an important molecule involved in vascular maintenance and homeostasis.[44,51] The Hsd11b1 cluster expressed a high level of homeostatic chemokine genes, *Cxcl14* and *Ccl11* (Figure 6C and Table S4), presumably helping maintain tissue homeostasis.[52,53] The two other clusters are specialized (Figures 5A, 6D, and S6A.1; Table S4). The Gdf10 cluster was enriched for genes involved in chondrogenesis, such as *Gdf10*, *Mgp*, *Prg4*, and *Cilp* (Figure 6D and Table S4). The pro-inflammatory cluster was very small (Figure S6B) and enriched for genes upregulated during inflammation, such as *Cxcl1*, *Ccl7*, and *Spp1* (Table S4). As skeletal muscle suffers constant micro-injuries due to mechanical stretch, the pro-inflammatory cluster may represent the FAPs that respond to micro-injuries. To infer the progression trajectories among FAP clusters, we did Monocle pseudotime trajectory analysis (Figure 5B). The Ly6c1^{hi}Pi16^{lo} cluster

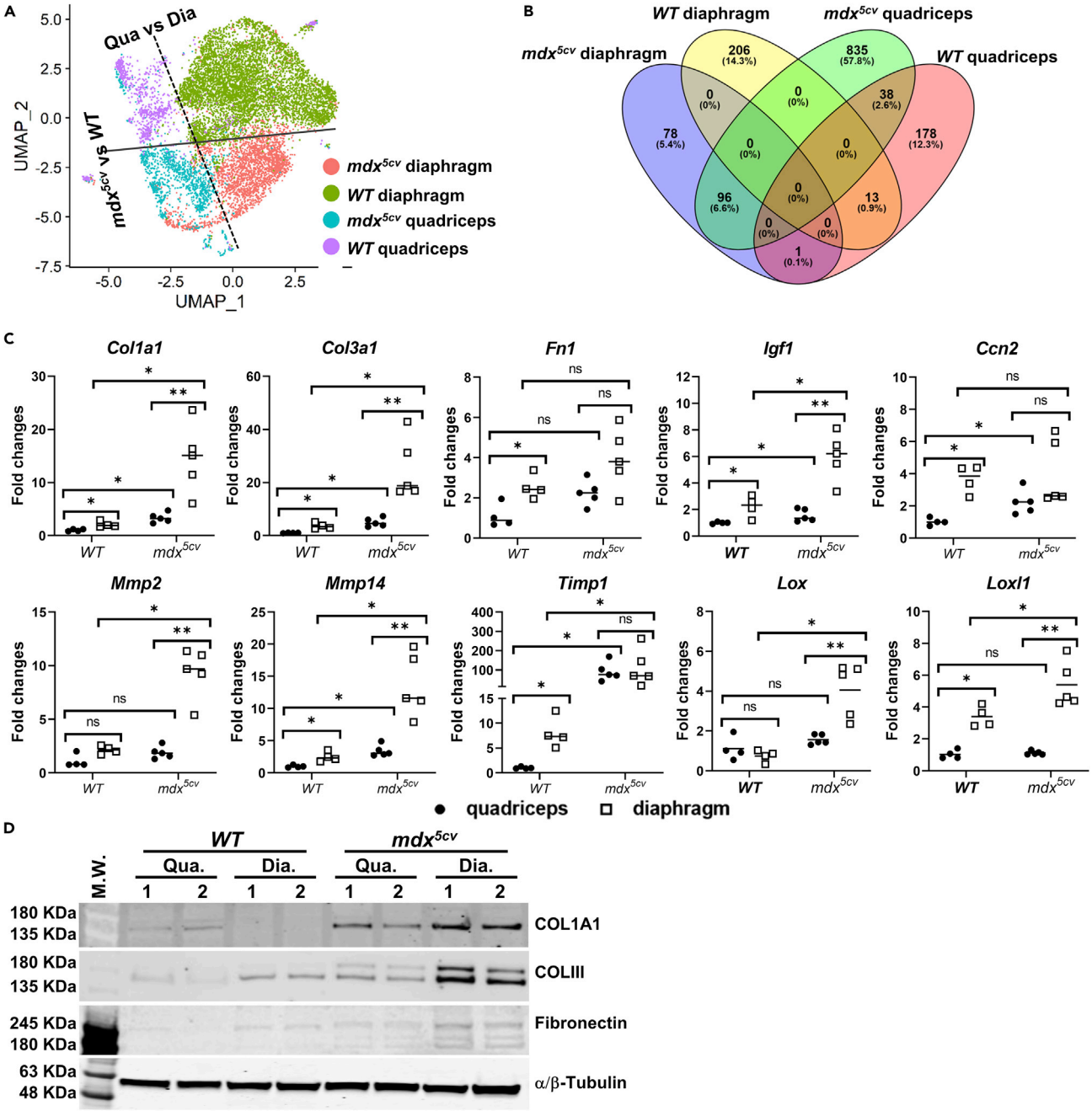

Figure 4. FAPs in *WT* and *mdx*^{5cv} diaphragm and quadriceps display differences in transcriptomes

(A) UMAP dimension reduction analysis showing different FAP transcriptomes in different muscle samples.

(B) Venn diagram depicting differentially expressed genes (DEGs) shared by or unique in FAPs of different muscles.

(C) qRT-PCR showing and comparing the expression of selected ECM and ECM regulatory genes by different muscles. Data are represented as mean ± SEM Asterisks indicate significant differences (*p < 0.05, **p < 0.01; ***p < 0.001, ns: no significance, Kruskal-Wallis test followed by Dunn's test for multiple comparisons). N = 5 mice/group.

(D) Western blot showing and comparing the protein expression of collagen 1α1 (COL1A1), collagen 3α1 (COL3A1), and fibronectin among different muscles. Results showed represent 3 independent experiments with a total of 6 mice for each group.

bridged the progression from the Ly6c1^{hi}Pi16^{hi} cluster to the Hsd11b1 cluster, and the two specialized clusters were directly from the Hsd11b1 cluster. The findings are consistent with the analysis of cross-tissue fibroblasts.[50]

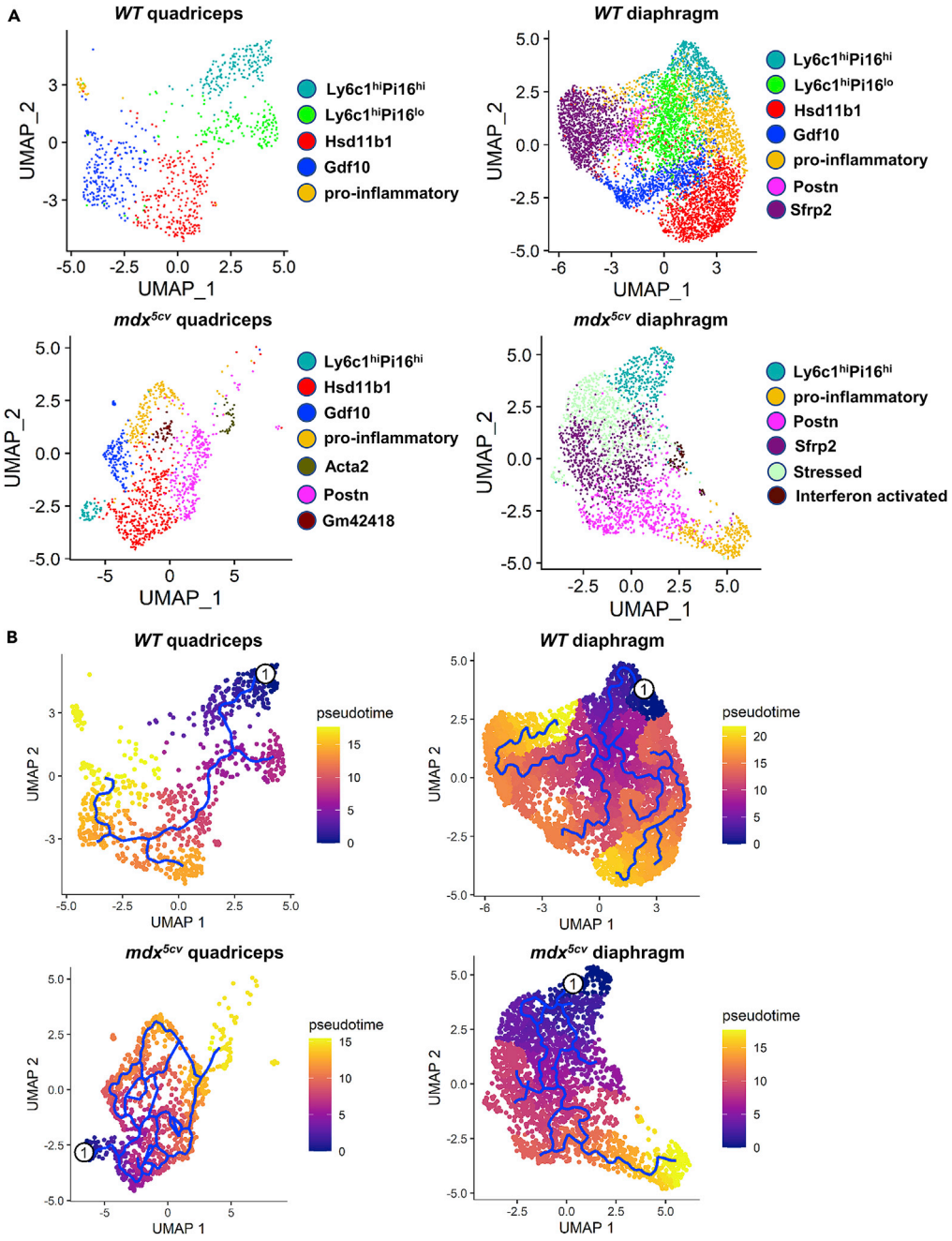

Figure 5. FAPs consist of diverse clusters which are different among quadriceps and diaphragm in *WT* and *mdx*^{5cv} mice

(A) UMAP clustering identifying FAP clusters in each muscle sample.

(B) Pseudotime analysis showing the trajectory of FAP differentiation starting from the Ly6c1^{hi}P16^{hi} cluster (labeled as 1) in each muscle sample.

Seven FAP clusters were identified in *WT* diaphragm, of which five were shared by *WT* quadriceps, including Ly6c1^{hi}Pi16^{hi}, Ly6c1^{hi}Pi16^{lo}, Hsd11b1, Gdf10, and pro-inflammatory clusters (Figures 5A, 6A-6D, and S6A.2; Table S5). But they all showed some differences in featured gene expression compared to their counterparts in *WT* quadriceps (Tables S4 and S5). The differential FAP specialization was further demonstrated by the presence of two additional FAP clusters in *WT* diaphragm: the Sfrp2 cluster and the

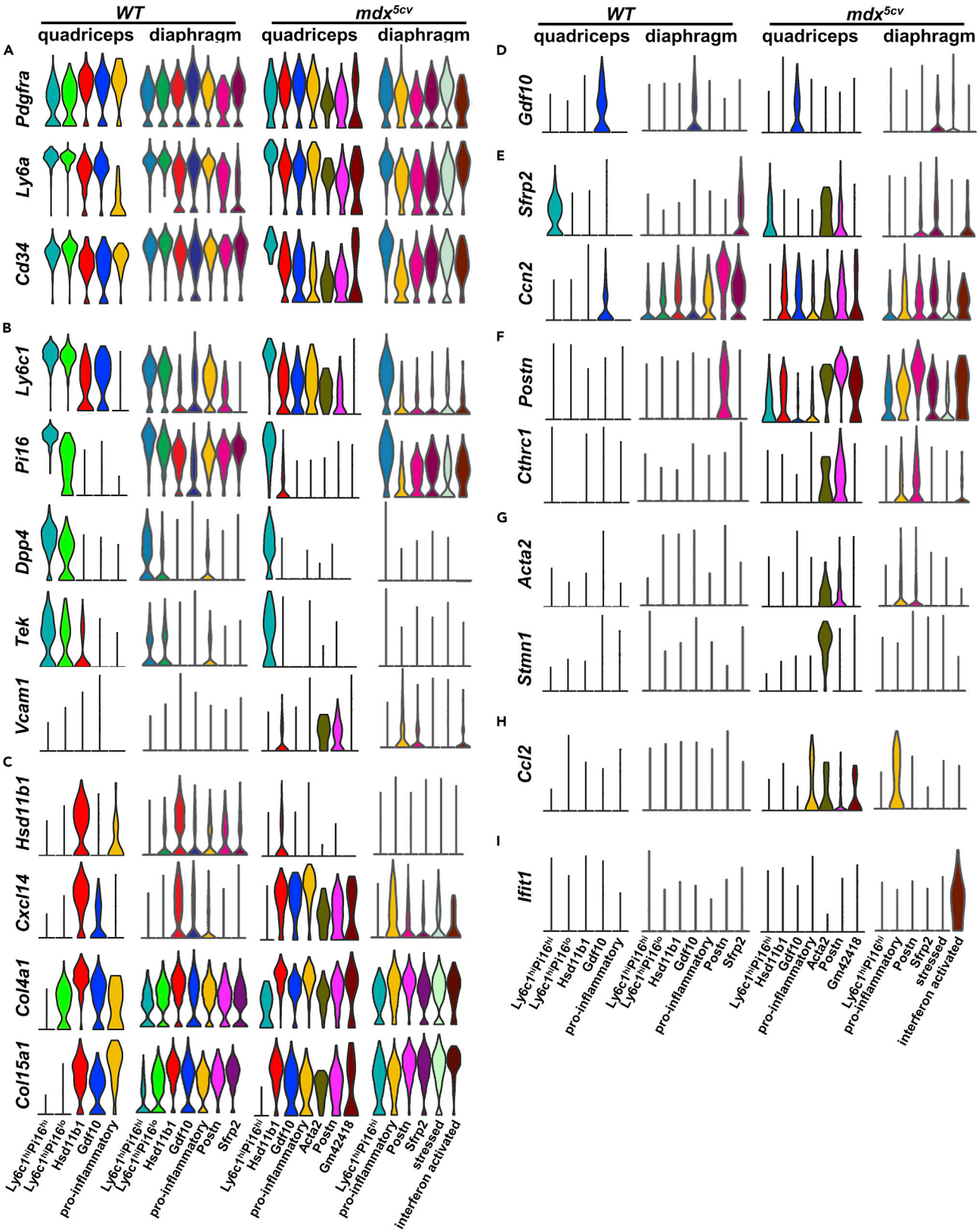
WT
mdx5cv
quadriceps
diaphragm
A
Pdgfra
Ly6a
Cd34
B
Ly6c1
Pi16
Dpp4
Tek
Vcam1
C
Hsd11b1
Cxcl14
Col4a1
Col15a1
Ly6c1hiPi16hi
Ly6c1hiPi16lo
Hsd11b1
Gdf10
pro-inflammatory
Postn
Sfrp2
Acta2
Gm42418
stressed
interferon activated
D
Gdf10
E
Sfrp2
Ccn2
F
Postn
Cthrc1
G
Acta2
Stmn1
H
Ccl2
I
Ifit1

Figure 6. FAP clusters show diverse gene expression depending on the muscle type and disease state

Violin plots showing gene expression by different FAP clusters in different muscle samples.

(A) FAP marker genes.

(B) Featured genes of Ly6c1^{hi} cluster.

(C) Featured genes of Hsd11b1 cluster.

(D) *Gdf10*.

(E) Featured genes of Sfrp2 cluster.

(F) Featured genes of Postn cluster.

(G) Featured genes of Acta2 cluster.

(H) *Ccl2*.

(I) *Ifit1*.

Postn cluster. The Sfrp2 cluster featured *Sfrp2* expression and enriched pro-fibrotic genes, including *Ccn2*, *Eln,* and *Mfap4* (Figure 6E and Table S5). The Postn cluster was also enriched for pro-fibrotic genes, including *Ccn2, Postn*, and *C1qtnf3* (Figures 6E and 6F and Table S5). Interestingly, *Sfrp2* was selectively expressed by the Ly6c1^{hi}Pi16^{hi} cluster in quadriceps while by the Sfrp2 cluster in diaphragm, (Figure 6E). *Sfrp2* gene encodes secreted frizzled-related protein 2 (SFRP2), which is an inhibitor of Wnt signaling and may regulate cell proliferation[54] and tissue fibrosis.[55,56] These findings suggest a generally higher pro-fibrotic microenvironment in diaphragm than in quadriceps, consistent with the higher FAP density in diaphragm than in quadriceps. In addition, the percentage of pro-inflammatory cluster increased dramatically in *WT* diaphragm as compared to *WT* quadriceps (Figure S6B), suggesting an increased level of micro-injuries in the steady state diaphragm. Pseudotime analysis showed that all the specialized clusters, in parallel with the Hsd11b1 cluster, were progressed from the Ly6c1^{hi}Pi16^{lo} cluster which was directly from the Ly6c1^{hi}Pi16^{hi} progenitor (Figure 5B).

Seven FAP clusters were identified in *mdx*^{5cv} quadriceps. Compared to *WT* quadriceps FAPs, the *mdx*^{5cv} quadriceps FAPs lost the Ly6c1^{hi}Pi16^{lo} intermediate universal cluster but acquired three new activated clusters: Postn, Acta2, and Gm42418 clusters (Figures 5A, 6A-6G, and S6A.3; Table S6). The Postn cluster was also enriched for *Ccn2, Postn*, and *C1qtnf3* as seen in *WT* diaphragm (Figures 6E and 6F and Table S6). The unique small Acta2 cluster featured the expression of *Acta2*, which encodes α-smooth muscle actin that is considered a marker of activated myofibroblasts.[57] This cluster was also enriched for genes involved in cell proliferation, including *Stmn1*, *Hmgb2*, and *S100a4* but not *Cdk* genes (Figure 6G and Table S6). Therefore, it may represent a cycling population of activated fibroblasts. The small Gm42418 cluster featured high expression of *Gm42418*, *Cd74*, and several ribosome protein genes (Table S6). Pro-fibrotic *Cthrc1*, which was not detectable in *WT* FAPs, was enriched in the Postn and Acta2 clusters (Figure 6F). The FAP expression of *Postn* and *Cthrc1* was also reported in acutely injured leg muscle.[36,46] *Vcam1*, a marker for pro-fibrotic FAPs,[44] was detected in the Hsd11b, Postn, and Acta2 clusters but not in *WT* FAPs (Figure 6B). The Ly6c1^{hi}Pi16^{hi}, Hsd11b1, Gdf10, and pro-inflammatory clusters in *mdx*^{5cv} quadriceps also showed profound changes in transcriptomes when compared to their counterparts in *WT* quadriceps (Tables S4 and S6). For instance, *Ccl2* expression was observed in the pro-inflammatory FAP cluster in *mdx*^{5cv} quadriceps but not in *WT* quadriceps or diaphragm (Figure 6H), and CCL2 mediates MO/MP infiltration in injured skeletal muscle.[58] Likewise, a subpopulation of FAPs in acutely injured muscle also expressed *Ccl2*.[46] Importantly, the relative abundance of the pro-inflammatory cluster was significantly increased, while the Ly6c1^{hi}Pi16^{hi} progenitor cluster was significantly decreased (Figure S6B). Along with the loss of the Ly6c1^{hi}Pi16^{lo} cluster, these changes indicate that the universal Ly6c1^{hi} clusters are greatly perturbed by muscular dystrophy, and they are differentiated into pro-inflammatory and pro-fibrotic clusters, corresponding to the inflammation and fibrosis seen in *mdx*^{5cv} quadriceps at 14 weeks of age (Figure S1). Pseudotime analysis showed that the Hsd11b1 cluster, progressed from the Ly6c1^{hi}Pi16^{hi} cluster, is the source of all the specialized and activated clusters (Figure 5B).

Mdx^{5cv} diaphragm FAPs contained six clusters, four of which were also present in *WT* diaphragm FAPs, including the Ly6c1^{hi}Pi16^{hi}, Sfrp2, Postn, and pro-inflammatory clusters (Figures 5A, 6, and S6A.4; Table S7). The Postn and pro-inflammatory clusters acquired the expression of pro-fibrotic *Vcam1*and *Cthrc1* (Figures 6B and 6F). As seen in *mdx*^{5cv} quadriceps, FAPs in *mdx*^{5cv} diaphragm did not contain the Ly6c1^{hi}Pi16^{lo} cluster. Compared to the other three samples, FAPs in *mdx*^{5cv} diaphragm showed substantial changes in clustering, including the loss of the universal Hsd11b1 cluster and the specialized Gdf10 cluster, and the presence of two distinct activated clusters: the stressed cluster and the interferon-activated cluster (Figures 5A, 6I, and S6A.4; Table S7). The stressed cluster was enriched for stress-response genes, including

Apod, *Egr1*, *Jun*, and *Hspa1b* (Table S7), a sign of increased tissue stress in *mdx*^{5cv} diaphragm. The interferon-activated cluster uniquely expressed interferon-response genes, including *Ifit1*, *Ifit3*, *Ligp1*, and *Cxcl9* (Figure 6I and Table S7), which was likely related to the significant *Ifng* expression by NK cells in *mdx*^{5cv} diaphragm (Figure 3A). Although this cluster is very small (Figure S6B), its unique presence suggests a different inflammatory microenvironment in *mdx*^{5cv} diaphragm than in *mdx*^{5cv} quadriceps. Pseudotime analysis showed a sequential progression: Ly6c1^{hi}Pi16^{hi} → Stressed → Sfrp2 → Postn → pro-inflammatory clusters, with the interferon-activated cluster progressed from the stressed cluster (Figure 5B).

Taken together, quadriceps and diaphragm FAPs are transcriptionally different, each containing unique specialized clusters in the steady state and distinct activated clusters in *mdx*^{5cv}, with more pro-fibrotic features present in the diaphragm FAPs than in the quadriceps FAPs.

Extracellular matrix and extracellular matrix regulatory genes are expressed by multiple Fibro/adipogenic progenitor clusters in *mdx*^{5cv} skeletal muscles

To further address the contributions of individual FAP clusters to the effector and regulatory functions related to skeletal muscle fibrosis in *mdx*^{5cv}, we analyzed the expression of the genes involved in ECM production and degradation by different FAP clusters in *mdx*^{5cv} diaphragm and quadriceps.

The Postn cluster expressed the highest level of most of the collagen genes in both quadriceps and diaphragm, including *Col1s* and *Col3s* (Figure 7A). *Fn1*, however, was preferentially expressed by the Ly6c1^{hi}Pi16^{hi} cluster (Figure 7A). Different proteoglycan genes were preferentially expressed by different FAP clusters (Figure 7B). *Ccn2* was preferentially expressed by the Sfrp2 cluster in diaphragm while was similarly expressed by several clusters in quadriceps (Figure 7C). The Hsd11b1 cluster in quadriceps and the Sfrp2 cluster in diaphragm expressed the highest level of *Mmp2* (Figure 7D). The quadriceps Acta2 cluster expressed a relatively high level of *Lox*s, especially *Loxl3* (Figure 7F). The Postn cluster in both muscles expressed the highest level of *Igf1*, *Mmp14*, and *Loxl1*, as well as a moderate level of *Lox*, *Loxl2*, and *Loxl3* (Figures 7C-7F). The pro-inflammatory cluster expressed the highest level of *Fst* and *Timp1* in both muscles (Figures 7C and 7E) and the highest level of *Lox* in diaphragm (Figure 7F). *Timp2* and *Timp3* were highly expressed by the Ly6c1^{hi}Pi16^{hi} cluster (Figure 7E). These findings suggest that the ECM production and degradation in *mdx*^{5cv} skeletal muscle may be regulated by multiple specialized and activated FAP clusters, and the Postn cluster appears the most pro-fibrotic one.

DISCUSSION

Fibrosis is a prominent pathological feature of skeletal muscle in patients with DMD and animal models, which directly contributes to muscle weakness.[3,4] FAPs are the main fibrogenic cells in skeletal muscle.[20,21] By scRNAseq analysis of intramuscular mononuclear cells derived from limb (quadriceps) and respiratory (diaphragm) muscles of both *WT* and *mdx*^{5cv} mice, our present study has generated several important findings, which deepens our understanding of the cellular and molecular mechanisms mediating and regulating skeletal muscle fibrosis.

First, despite more severe and progressive fibrosis seen in *mdx*^{5cv} diaphragm than in *mdx*^{5cv} quadriceps, the expression of most ECM genes by FAPs at a single-cell level is not different between these two muscles. But the ECM gene and protein expression at a whole-muscle level is significantly higher in *mdx*^{5cv} diaphragm than in *mdx*^{5cv} quadriceps. Since FAPs are the primary source of ECM in skeletal muscle, the relatively high ECM gene expression in *mdx*^{5cv} diaphragm is most likely contributed by the high abundance of FAPs in this muscle. It remains possible that the ECM protein degradation may also be different between *mdx*^{5cv} diaphragm and quadriceps.

The difference in the FAP density between *mdx*^{5cv} quadriceps and diaphragm is prominent. It could be in part intrinsic to the muscle type, as the FAP density is much higher in *WT* diaphragm than in *WT* quadriceps. Interestingly, the percentages of proliferating and apoptotic FAPs are both higher in *mdx*^{5cv} quadriceps than in *mdx*^{5cv} diaphragm (Figures S7A and S7B), indicating a higher FAP turnover in *mdx*^{5cv} quadriceps than in *mdx*^{5cv} diaphragm. The expression of the FAP senescence genes, including *Cdkn1a*, *Cdkn2a*, *Trp53*, and *Fas*,[59] is low in both *mdx*^{5cv} quadriceps and diaphragm FAPs (Figure S7C). Apoptosis, proliferation, and fibrogenic function of FAPs are regulated by TNF-α and TGF-β signaling. While TNF-α signaling induces FAP apoptosis, TGF-β signaling inhibits FAP apoptosis,[25] and it also promotes FAP proliferation and fibrogenic differentiation.[34,35,60] While TGF-β signaling is enriched in the DEGs of both *mdx*^{5cv}

Figure 7. ECM genes and ECM regulatory genes are expressed by multiple FAP clusters

(A–F) Dot plot showing the expression of collagen and fibronectin genes (A), proteoglycan genes (B), fibrogenic factor genes (C), *Mmps* (D), *Timps* (E), and *Loxs* (F) by FAP clusters of *mdx*^{5cv} quadriceps and diaphragm.

diaphragm and quadriceps FAPs, TNF-α signaling is enriched only in the *mdx*^{5cv} quadriceps FAPs. The difference might contribute, in part, to the persistent high number of FAPs in *mdx*^{5cv} diaphragm.

Second, our study supports the notion that FAPs are not only important effectors but also the master regulators of ECM homeostasis and fibrosis in skeletal muscle. FAPs are known primary ECM producers. Our

study further suggests that FAPs may also be the critical regulators of ECM production and degradation, as they may regulate many aspects of skeletal muscle fibrogenesis by expressing *Ccn2*, *Ltbp4*, *Mmp2*, *Mmp14*, *Timp1*, *Timp2*, and *Loxs*.

Fibrosis is the end result of chronic inflammation, and the two potent pro-fibrogenic genes, *Tgfb1* and *Spp1*, are mainly expressed by MOs/MPs in *mdx*^{5cv} muscles. But *Ltbp4*, an important regulatory gene of TGF-β bioavailability[61] and a genetic modifier of DMD mice and humans,[62–65] is predominantly expressed by FAPs. FAPs also express TGF-β1, TGF-β2, and TGF-β3, which can promote their own fibrogenic differentiation.[24] Another important pro-fibrogenic growth factor, CTGF, is highly expressed by FAPs. CTGF stimulates *Col1*, *Col3*, and *Fn* expression. *Ccn2* overexpression in mice caused dystrophic changes,[66] while CTGF inhibition in *mdx* reduced muscle fibrosis without affecting TGF-β signaling.[67] Interestingly, a recent study showed that CTGF, derived from myofibers but not fibroblasts, affected collagen content and organization, contributing to muscular dystrophy in δ-sarcoglycan-null mice.[38] The role of FAP-derived CTGF in *mdx*^{5cv} needs to be further determined. FAPs are also the major cells that express the IGF-1 and follistatin genes, regulating not only muscle fibrosis but also muscle regeneration.

MMPs and TIMPs are multifunctional proteins, regulating inflammation, fibrogenesis, myogenesis, and angiogenesis in skeletal muscle via controlling the degradation of ECM and the activation of growth factors and cell adhesion molecules.[17,68] Of the three *Mmps* that are highly expressed by skeletal muscle mononuclear cells, two are highly expressed by FAPs, including *Mmp2* and *Mmp14*. *Mmp9* is mainly expressed by neutrophils. These MMPs play a key role in collagen and fibronectin degradation, which can limit fibrosis. On the other hand, MMP-9 and MMP-14 can also promote fibrosis by cleaving and activating latent TGF-β1 and CTGF.[69,70] They are double-edged swords. Although MMP-14 has been implicated in promoting adipogenic differentiation of FAPs,[71,72] the expression of the adipogenic genes, including *Pparg*, *Fabp4*, *Adipoq*, and *Cebpa*, is barely detectable in *mdx*^{5cv} FAPs (Figure S7D). MMP-14, along with TIMP2, activates MMP-2, and both MMPs are critically involved in skeletal muscle maturation.[17,68,73–75] Ablation of MMP-2 in *mdx* impaired muscle regeneration and angiogenesis.[76] The role of MMP-14 in *mdx* has not been well studied. Given the diverse functions of this membrane-bound MMP, the overall role of the FAP-derived MMP-14 in *mdx*^{5cv} is difficult to predict and needs to be further determined.

TIMPs inhibit the proteolytic activity of MMPs. Among the four TIMP genes, *Timp1* and *Timp2* are mainly expressed by FAPs. FAPs are thus likely the significant contributors to the elevated TIMP-1 and TIMP-2 levels in the plasma and skeletal muscles of patients with DMD and animal models.[77–80] TIMP-1 and TIMP-2 can promote fibrosis not only by reducing ECM proteolysis but also by stimulating fibrogenic cell proliferation and collagen production.[17] FAP-derived TIMPs may thus contribute significantly to the skeletal muscle fibrosis in *mdx*^{5cv}. Being the major cells that express *Timp3* and *Timp4*, ECs may regulate FAP differentiation, as *Timp3* inhibits adipogenic differentiation of FAPs.[72,81,82]

The important regulatory functions of FAPs are further exemplified by their significant expression of *Loxs* for collagen cross-linking. FAPs, therefore, may regulate the mechanical properties of ECM and contribute to the increased collagen cross-linking detected in skeletal muscles of patients with DMD and animal models.[19] Taken together, FAPs appear critically involved in the regulation of skeletal muscle fibrosis in *mdx*^{5cv}. FAPs may also regulate inflammation, regeneration, and angiogenesis associated with muscular dystrophy via their predominant expression of important growth factors, *Mmps*, and *Timps*.

Third, our study demonstrates the presence of FAP clusters specialized by muscle type in the steady state, limb (quadriceps) muscle vs. respiratory (diaphragm) muscle. While FAPs in both muscles contain the universal adventitia-associated Ly6c1^{hi} clusters and basement membrane-associated Hsd11b1 cluster and share the specialized Gdf10 and pro-inflammatory clusters, the diaphragm FAPs also contains the uniquely specialized Postn and Sfrp2 clusters. Based on the enriched genes in the muscle type-specific FAP clusters, the diaphragm appears to have an increased level of micro-injury and a generally high pro-fibrotic microenvironment compared to the quadriceps. Likewise, muscle type-specific clusters have also been identified in the steady state resident macrophages, which also suggests an increased level of micro-injury in diaphragm as compared to quadriceps.[83] The intrinsic differences in tissue microenvironment may be related to the different structural origins that limb and diaphragm muscles arise from during embryonic development,[22] and they may contribute, in part, to the differential responses to a variety of muscle diseases. While some muscle diseases affect both limb and respiratory muscles, others preferentially affect limb or respiratory muscles.

Fourth, *mdx*^{5cv} diaphragm and quadriceps FAPs respond differently to muscular dystrophy, with more profound changes seen in the FAP clustering in the diaphragm than in the quadriceps. Both universal and specialized clusters are greatly perturbed by the muscular dystrophy in *mdx*^{5cv}. While FAPs in both muscles lose the intermediate Ly6c1^{hi}Pi16^{lo} cluster, FAPs in *mdx*^{5cv} diaphragm also lose the universal Hsd11b1 cluster and the specialized Gdf10 cluster. *Hsd11b1* encodes 11b-Hydroxysteroid Dehydrogenase 1, which has been implicated in suppressing fibrosis, as deficiency or inhibition of this enzyme promotes fibroblast activation and enhances fibrosis in liver and skin.[84,85] The Hsd11b1 cluster is thus likely differentiated into more pro-fibrotic clusters in *mdx*^{5cv} diaphragm. The selective loss of the Hsd11b1 cluster in *mdx*^{5cv} diaphragm also suggests more severe perturbation of tissue homeostasis in *mdx*^{5cv} diaphragm than in *mdx*^{5cv} quadriceps, as this cluster is enriched for homeostatic chemokine genes. PDGFRα^{+} mesenchymal progenitors-derived GDF10 has been shown to maintain skeletal muscle integrity[86] and suppress adipogenic differentiation of FAPs.[49] The loss of this cluster may suggest its differentiation into pathogenic clusters to contribute to muscular dystrophy in *mdx*^{5cv} diaphragm. *Mdx*^{5cv} diaphragm acquires two uniquely activated clusters: the stressed cluster and the interferon-activated cluster. The presence of the stressed cluster suggests exceptionally high stress in the microenvironment of *mdx*^{5cv} diaphragm. Since many stress-responsive genes are also potent pro-inflammatory genes, such as *Egr1* and *Jun*,[87,88] the presence of the stressed cluster also indicates a high pro-inflammatory microenvironment in *mdx*^{5cv} diaphragm. The unique presence of the interferon-activated FAP cluster further supports a special inflammatory microenvironment in *mdx*^{5cv} diaphragm. These two uniquely activated clusters likely contribute to the persistent inflammation and progressive fibrosis in *mdx*^{5cv} diaphragm.

In summary, our study supports the critical roles of FAPs in skeletal muscle ECM homeostasis and fibrosis, both as predominant effectors and crucial regulators. The persistent high abundance of FAPs appears the main contributor to the progressive fibrosis in *mdx*^{5cv} diaphragm. Limb and diaphragm muscles have different embryonic origins, locate at different anatomical positions, and work under different mechanical stress. These differences likely drive the differential FAP specialization in the steady state and differential FAP activation in muscular dystrophy. The high pro-fibrotic microenvironment likely contributes to the persistent high FAP abundance and progressive fibrosis in *mdx*^{5cv} diaphragm. The anti-fibrotic therapy development for DMD should target not only the ECM production but also the pro-fibrogenic regulatory functions of FAPs.

Limitations of the study

Since polynuclear myofibers cannot be included in single-cell suspensions for scRNAseq or FACS sorting due to their large size, their expression of the ECM and ECM regulatory genes cannot be directly assessed or compared with FAPs. Future snRNAseq can help circumvent the difficulty. scRNAseq cannot assess locations of FAPs in dystrophic muscle, while spatial transcriptomics can (https://www.biorxiv.org/content/10.1101/2022.03.17.484699v1.full.pdf). Future spatial transcriptomics studies will be helpful to localize different FAP clusters and correlate with histopathological changes in dystrophic muscle. Our scRNAseq is performed using the mice at 14 weeks of age, after which *mdx*^{5cv} diaphragm and limb muscles undergo divergent fibrosis progression. Future studies at later time points may help identify additional differences in FAP transcriptomes that underlie the divergent fibrosis progression. Our study has identified several regulatory genes of fibrosis that are predominantly expressed by FAPs. Future studies with FAP-specific deletion are needed to verify the functional importance of the FAP expression of these genes in muscular dystrophy.

STAR★METHODS

Detailed methods are provided in the online version of this paper and include the following:

- KEY RESOURCES TABLE
- RESOURCE AVAILABILITY
  - Lead contact
  - Materials availability
  - Data and code availability
- EXPERIMENTAL MODEL AND SUBJECT DETAILS
  - Animals
- METHOD DETAILS
  - Muscle sample collection
  - Histopathological analysis

- Muscle single-cell suspension preparation
- Flow cytometry analysis and cell sorting
- FAP apoptosis assay
- FAP proliferation assay
- RNA preparation and qRT-PCR
- Western blot
- Single-cell cDNA library preparation and sequencing
- Single cell-based mRNA sequencing analysis
- Functional enrichment analysis
- Pseudotime trajectory analysis
- Venn diagram

● QUANTIFICATION AND STATISTICAL ANALYSIS

SUPPLEMENTAL INFORMATION

Supplemental information can be found online at https://doi.org/10.1016/j.isci.2022.105775.

ACKNOWLEDGMENTS

Research reported in this publication was supported by the National Institute of Arthritis And Musculoskeletal and Skin Diseases of the National Institutes of Health under Award Number 1R01AR074428 (LZ). The content is solely the responsibility of the authors and does not necessarily represent the official views of the National Institutes of Health.

AUTHOR CONTRIBUTIONS

XW: Conducted the experiments, analyzed the data, made the figures, and wrote the article. JC: Analyzed the scRNAseq data, conducted the experiments, and made the figures. SH: Conducted the experiments. YW: Conducted the experiments. GRS: Analyzed the scRNAseq data. FRZ: Conducted the scRNAseq experiment. SCS: Supervised the scRNAseq experiment. LZ: Designed the study, analyzed the data, and wrote the article.

DECLARATION OF INTERESTS

All the authors have no conflict of interest to report.

Received: April 20, 2022
Revised: September 8, 2022
Accepted: December 6, 2022
Published: January 20, 2023

REFERENCES

1. Duan, D., Goemans, N., Takeda, S., Mercuri, E., and Aartsma-Rus, A. (2021). Duchenne muscular dystrophy. Nat. Rev. Dis. Primers *7*, 13. https://doi.org/10.1038/s41572-021-00248-3.

2. Ryder, S., Leadley, R.M., Armstrong, N., Westwood, M., de Kock, S., Butt, T., Jain, M., and Kleijnen, J. (2017). The burden, epidemiology, costs and treatment for Duchenne muscular dystrophy: an evidence review. Orphanet J. Rare Dis. *12*, 79. https://doi.org/10.1186/s13023-017-0631-3.

3. Desguerre, I., Mayer, M., Leturcq, F., Barbet, J.P., Gherardi, R.K., and Christov, C. (2009). Endomysial fibrosis in Duchenne muscular dystrophy: a marker of poor outcome associated with macrophage alternative activation. J. Neuropathol. Exp. Neurol. *68*, 762–773. https://doi.org/10.1097/NEN.0b013e3181aa31c2.

4. Klingler, W., Jurkat-Rott, K., Lehmann-Horn, F., and Schleip, R. (2012). The role of fibrosis in Duchenne muscular dystrophy. Acta Myol. *31*, 184–195.

5. Beastrom, N., Lu, H., Macke, A., Canan, B.D., Johnson, E.K., Penton, C.M., Kaspar, B.K., Rodino-Klapac, L.R., Zhou, L., Janssen, P.M.L., and Montanaro, F. (2011). mdx((5)cv) mice manifest more severe muscle dysfunction and diaphragm force deficits than do mdx Mice. Am. J. Pathol. *179*, 2464–2474. https://doi.org/10.1016/j.ajpath.2011.07.009.

6. Dupont-Versteegden, E.E., and McCarter, R.J. (1992). Differential expression of muscular dystrophy in diaphragm versus hindlimb muscles of mdx mice. Muscle Nerve *15*, 1105–1110. https://doi.org/10.1002/mus.880151008.

7. Stedman, H.H., Sweeney, H.L., Shrager, J.B., Maguire, H.C., Panettieri, R.A., Petrof, B., Narusawa, M., Leferovich, J.M., Sladky, J.T., and Kelly, A.M. (1991). The mdx mouse diaphragm reproduces the degenerative changes of Duchenne muscular dystrophy. Nature *352*, 536–539. https://doi.org/10.1038/352536a0.

8. Zhou, L., Porter, J.D., Cheng, G., Gong, B., Hatala, D.A., Merriam, A.P., Zhou, X., Rafael, J.A., and Kaminski, H.J. (2006). Temporal and spatial mRNA expression patterns of TGF-beta1, 2, 3 and TbetaRI, II, III in skeletal muscles of mdx mice. Neuromuscul. Disord. *16*, 32–38. https://doi.org/10.1016/j.nmd.2005.09.009.

9. Csapo, R., Gumpenberger, M., and Wessner, B. (2020). Skeletal muscle extracellular matrix - what do we know about its composition, regulation, and physiological roles? A

narrative review. Front. Physiol. *11*, 253. https://doi.org/10.3389/fphys.2020.00253.

10. Gillies, A.R., and Lieber, R.L. (2011). Structure and function of the skeletal muscle extracellular matrix. Muscle Nerve *44*, 318–331. https://doi.org/10.1002/mus.22094.

11. Zhang, W., Liu, Y., and Zhang, H. (2021). Extracellular matrix: an important regulator of cell functions and skeletal muscle development. Cell Biosci. *11*, 65. https://doi.org/10.1186/s13578-021-00579-4.

12. Ismaeel, A., Kim, J.S., Kirk, J.S., Smith, R.S., Bohannon, W.T., and Koutakis, P. (2019). Role of transforming growth factor-beta in skeletal muscle fibrosis: a review. Int. J. Mol. Sci. *20*, 2446. https://doi.org/10.3390/ijms20102446.

13. Rebolledo, D.L., Lipson, K.E., and Brandan, E. (2021). Driving fibrosis in neuromuscular diseases: role and regulation of connective tissue growth factor (CCN2/CTGF). Matrix Biol. *11*, 100059. https://doi.org/10.1016/j.mbplus.2021.100059.

14. Pagel, C.N., Wasgewatte Wijesinghe, D.K., Taghavi Esfandouni, N., and Mackie, E.J. (2014). Osteopontin, inflammation and myogenesis: influencing regeneration, fibrosis and size of skeletal muscle. J. Cell Commun. Signal. *8*, 95–103. https://doi.org/10.1007/s12079-013-0217-3.

15. Kramerova, I., Kumagai-Cresse, C., Ermolova, N., Mokhonova, E., Marinov, M., Capote, J., Becerra, D., Quattrocelli, M., Crosbie, R.H., Welch, E., et al. (2019). Spp1 (osteopontin) promotes TGFbeta processing in fibroblasts of dystrophin-deficient muscles through matrix metalloproteinases. Hum. Mol. Genet. *28*, 3431–3442. https://doi.org/10.1093/hmg/ddz181.

16. Vetrone, S.A., Montecino-Rodriguez, E., Kudryashova, E., Kramerova, I., Hoffman, E.P., Liu, S.D., Miceli, M.C., and Spencer, M.J. (2009). Osteopontin promotes fibrosis in dystrophic mouse muscle by modulating immune cell subsets and intramuscular TGF-beta. J. Clin. Invest. *119*, 1583–1594. https://doi.org/10.1172/JCI37662.

17. Alameddine, H.S., and Morgan, J.E. (2016). Matrix metalloproteinases and tissue inhibitor of metalloproteinases in inflammation and fibrosis of skeletal muscles. J. Neuromuscul. Dis. *3*, 455–473. https://doi.org/10.3233/JND-160183.

18. Afratis, N.A., Klepfish, M., Karamanos, N.K., and Sagi, I. (2018). The apparent competitive action of ECM proteases and cross-linking enzymes during fibrosis: applications to drug discovery. Adv. Drug Deliv. Rev. *129*, 4–15. https://doi.org/10.1016/j.addr.2018.03.004.

19. Smith, L.R., Hammers, D.W., Sweeney, H.L., and Barton, E.R. (2016). Increased collagen cross-linking is a signature of dystrophin-deficient muscle. Muscle Nerve *54*, 71–78. https://doi.org/10.1002/mus.24998.

20. Joe, A.W.B., Yi, L., Natarajan, A., Le Grand, F., So, L., Wang, J., Rudnicki, M.A., and Rossi, F.M.V. (2010). Muscle injury activates resident fibro/adipogenic progenitors that facilitate myogenesis. Nat. Cell Biol. *12*, 153–163. https://doi.org/10.1038/ncb2015.

21. Uezumi, A., Ito, T., Morikawa, D., Shimizu, N., Yoneda, T., Segawa, M., Yamaguchi, M., Ogawa, R., Matev, M.M., Miyagoe-Suzuki, Y., et al. (2011). Fibrosis and adipogenesis originate from a common mesenchymal progenitor in skeletal muscle. J. Cell Sci. *124*, 3654–3664. https://doi.org/10.1242/jcs.086629.

22. Contreras, O., Rossi, F.M.V., and Theret, M. (2021). Origins, potency, and heterogeneity of skeletal muscle fibro-adipogenic progenitors-time for new definitions. Skelet. Muscle *11*, 16. https://doi.org/10.1186/s13395-021-00265-6.

23. Theret, M., Rossi, F.M.V., and Contreras, O. (2021). Evolving roles of muscle-resident fibro-adipogenic progenitors in Health, regeneration, neuromuscular disorders, and aging. Front. Physiol. *12*, 673404. https://doi.org/10.3389/fphys.2021.673404.

24. Contreras, O., Cruz-Soca, M., Theret, M., Soliman, H., Tung, L.W., Groppa, E., Rossi, F.M., and Brandan, E. (2019). Cross-talk between TGF-beta and PDGFRalpha signaling pathways regulates the fate of stromal fibro-adipogenic progenitors. J. Cell Sci. *132*, jcs232157. https://doi.org/10.1242/jcs.232157.

25. Lemos, D.R., Babaeijandaghi, F., Low, M., Chang, C.K., Lee, S.T., Fiore, D., Zhang, R.H., Natarajan, A., Nedospasov, S.A., and Rossi, F.M.V. (2015). Nilotinib reduces muscle fibrosis in chronic muscle injury by promoting TNF-mediated apoptosis of fibro/adipogenic progenitors. Nat. Med. *21*, 786–794. https://doi.org/10.1038/nm.3869.

26. Heredia, J.E., Mukundan, L., Chen, F.M., Mueller, A.A., Deo, R.C., Locksley, R.M., Rando, T.A., and Chawla, A. (2013). Type 2 innate signals stimulate fibro/adipogenic progenitors to facilitate muscle regeneration. Cell *153*, 376–388. https://doi.org/10.1016/j.cell.2013.02.053.

27. Mozzetta, C., Consalvi, S., Saccone, V., Tierney, M., Diamantini, A., Mitchell, K.J., Marazzi, G., Borsellino, G., Battistini, L., Sassoon, D., et al. (2013). Fibroadipogenic progenitors mediate the ability of HDAC inhibitors to promote regeneration in dystrophic muscles of young, but not old Mdx mice. EMBO Mol. Med. *5*, 626–639. https://doi.org/10.1002/emmm.201202096.

28. Wosczyna, M.N., Konishi, C.T., Perez Carbajal, E.E., Wang, T.T., Walsh, R.A., Gan, Q., Wagner, M.W., and Rando, T.A. (2019). Mesenchymal stromal cells are required for regeneration and homeostatic maintenance of skeletal muscle. Cell Rep. *27*, 2029–2035.e5. https://doi.org/10.1016/j.celrep.2019.04.074.

29. Urciuolo, A., Quarta, M., Morbidoni, V., Gattazzo, F., Molon, S., Grumati, P., Montemurro, F., Tedesco, F.S., Blaauw, B., Cossu, G., et al. (2013). Collagen VI regulates satellite cell self-renewal and muscle regeneration. Nat. Commun. *4*, 1964. https://doi.org/10.1038/ncomms2964.

30. Zhao, W., Wang, X., Ransohoff, R.M., and Zhou, L. (2017). CCR2 deficiency does not provide sustained improvement of muscular dystrophy in mdx5cv mice. FASEB J. *31*, 35–46. https://doi.org/10.1096/fj.201600619R.

31. Stuart, T., Butler, A., Hoffman, P., Hafemeister, C., Papalexi, E., Mauck, W.M., 3rd, Hao, Y., Stoeckius, M., Smibert, P., and Satija, R. (2019). Comprehensive integration of single-cell data. Cell *177*, 1888–1902.e21. https://doi.org/10.1016/j.cell.2019.05.031.

32. Mutsaers, S.E. (2002). Mesothelial cells: their structure, function and role in serosal repair. Respirology *7*, 171–191. https://doi.org/10.1046/j.1440-1843.2002.00404.x.

33. Contreras, O., Rebolledo, D.L., Oyarzún, J.E., Olguín, H.C., and Brandan, E. (2016). Connective tissue cells expressing fibro/adipogenic progenitor markers increase under chronic damage: relevance in fibroblast-myofibroblast differentiation and skeletal muscle fibrosis. Cell Tissue Res. *364*, 647–660. https://doi.org/10.1007/s00441-015-2343-0.

34. Contreras, O., Rossi, F.M., and Brandan, E. (2019). Adherent muscle connective tissue fibroblasts are phenotypically and biochemically equivalent to stromal fibro/adipogenic progenitors. Matrix Biol. *2*, 100006. https://doi.org/10.1016/j.mbplus.2019.04.003.

35. Contreras, O., Soliman, H., Theret, M., Rossi, F.M.V., and Brandan, E. (2020). TGF-beta-driven downregulation of the transcription factor TCF7L2 affects Wnt/beta-catenin signaling in PDGFRalpha(+) fibroblasts. J. Cell Sci. *133*, jcs242297. https://doi.org/10.1242/jcs.242297.

36. Scott, R.W., Arostegui, M., Schweitzer, R., Rossi, F.M.V., and Underhill, T.M. (2019). Hic1 defines quiescent mesenchymal progenitor subpopulations with distinct functions and fates in skeletal muscle regeneration. Cell Stem Cell *25*, 797–813.e9. https://doi.org/10.1016/j.stem.2019.11.004.

37. Mahdy, M.A.A. (2019). Skeletal muscle fibrosis: an overview. Cell Tissue Res. *375*, 575–588. https://doi.org/10.1007/s00441-018-2955-2.

38. Petrosino, J.M., Leask, A., and Accornero, F. (2019). Genetic manipulation of CCN2/CTGF unveils cell-specific ECM-remodeling effects in injured skeletal muscle. FASEB J. *33*, 2047–2057. https://doi.org/10.1096/fj.201800622RR.

39. Reggio, A., Rosina, M., Palma, A., Cerquone Perpetuini, A., Petrilli, L.L., Gargioli, C., Fuoco, C., Micarelli, E., Giuliani, G., Cerretani, M., et al. (2020). Adipogenesis of skeletal muscle fibro/adipogenic progenitors is affected by the WNT5a/GSK3/beta-catenin axis. Cell Death Differ. *27*, 2921–2941. https://doi.org/10.1038/s41418-020-0551-y.

40. Tidball, J.G., Welc, S.S., and Wehling-Henricks, M. (2018). Immunobiology of inherited muscular dystrophies. Compr. Physiol. *8*, 1313–1356. https://doi.org/10.1002/cphy.c170052.

41. Juban, G., Saclier, M., Yacoub-Youssef, H., Kernou, A., Arnold, L., Boisson, C., Ben Larbi, S., Magnan, M., Cuvellier, S., Théret, M., et al. (2018). AMPK activation regulates LTBP4-dependent TGF-beta1 secretion by pro-inflammatory macrophages and controls fibrosis in Duchenne muscular dystrophy. Cell Rep. *25*, 2163–2176.e6. https://doi.org/10.1016/j.celrep.2018.10.077.

42. Contreras, O., Córdova-Casanova, A., and Brandan, E. (2021). PDGF-PDGFR network differentially regulates the fate, migration, proliferation, and cell cycle progression of myogenic cells. Cell. Signal. *84*, 110036. https://doi.org/10.1016/j.cellsig.2021.110036.

43. Uezumi, A., Ikemoto-Uezumi, M., and Tsuchida, K. (2014). Roles of nonmyogenic mesenchymal progenitors in pathogenesis and regeneration of skeletal muscle. Front. Physiol. *5*, 68. https://doi.org/10.3389/fphys.2014.00068.

44. Malecova, B., Gatto, S., Etxaniz, U., Passafaro, M., Cortez, A., Nicoletti, C., Giordani, L., Torcinaro, A., De Bardi, M., Bicciato, S., et al. (2018). Dynamics of cellular states of fibro-adipogenic progenitors during myogenesis and muscular dystrophy. Nat. Commun. *9*, 3670. https://doi.org/10.1038/s41467-018-06068-6.

45. Mázala, D.A., Novak, J.S., Hogarth, M.W., Nearing, M., Adusumalli, P., Tully, C.B., Habib, N.F., Gordish-Dressman, H., Chen, Y.W., Jaiswal, J.K., and Partridge, T.A. (2020). TGF-beta-driven muscle degeneration and failed regeneration underlie disease onset in a DMD mouse model. JCI Insight *5*, e135703. https://doi.org/10.1172/jci.insight.135703.

46. Oprescu, S.N., Yue, F., Qiu, J., Brito, L.F., and Kuang, S. (2020). Temporal dynamics and heterogeneity of cell populations during skeletal muscle regeneration. iScience *23*, 100993. https://doi.org/10.1016/j.isci.2020.100993.

47. Giuliani, G., Vumbaca, S., Fuoco, C., Gargioli, C., Giorda, E., Massacci, G., Palma, A., Reggio, A., Riccio, F., Rosina, M., et al. (2021). SCA-1 micro-heterogeneity in the fate decision of dystrophic fibro/adipogenic progenitors. Cell Death Dis. *12*, 122. https://doi.org/10.1038/s41419-021-03408-1.

48. Stumm, J., Vallecillo-García, P., Vom Hofe-Schneider, S., Ollitrault, D., Schrewe, H., Economides, A.N., Marazzi, G., Sassoon, D.A., and Stricker, S. (2018). Odd skipped-related 1 (Osr1) identifies muscle-interstitial fibro-adipogenic progenitors (FAPs) activated by acute injury. Stem Cell Res. *32*, 8–16. https://doi.org/10.1016/j.scr.2018.08.010.

49. Camps, J., Breuls, N., Sifrim, A., Giarratana, N., Corvelyn, M., Danti, L., Grosemans, H., Vanuytven, S., Thiry, I., Belicchi, M., et al. (2020). Interstitial cell remodeling promotes aberrant adipogenesis in dystrophic muscles. Cell Rep. *31*, 107597. https://doi.org/10.1016/j.celrep.2020.107597.

50. Buechler, M.B., Pradhan, R.N., Krishnamurty, A.T., Cox, C., Calviello, A.K., Wang, A.W., Yang, Y.A., Tam, L., Caothien, R., Roose-Girma, M., et al. (2021). Cross-tissue organization of the fibroblast lineage. Nature *593*, 575–579. https://doi.org/10.1038/s41586-021-03549-5.

51. Fiedler, U., and Augustin, H.G. (2006). Angiopoietins: a link between angiogenesis and inflammation. Trends Immunol. *27*, 552–558. https://doi.org/10.1016/j.it.2006.10.004.

52. Marichal, T., Mesnil, C., and Bureau, F. (2017). Homeostatic eosinophils: characteristics and functions. Front. Med. *4*, 101. https://doi.org/10.3389/fmed.2017.00101.

53. Kouzeli, A., Collins, P.J., Metzemaekers, M., Meyrath, M., Szpakowska, M., Artinger, M., Struyf, S., Proost, P., Chevigne, A., Legler, D.F., et al. (2020). CXCL14 preferentially synergizes with homeostatic chemokine receptor systems. Front. Immunol. *11*, 561404. https://doi.org/10.3389/fimmu.2020.561404.

54. van Loon, K., Huijbers, E.J.M., and Griffioen, A.W. (2021). Secreted frizzled-related protein 2: a key player in noncanonical Wnt signaling and tumor angiogenesis. Cancer Metastasis Rev. *40*, 191–203. https://doi.org/10.1007/s10555-020-09941-3.

55. Kobayashi, K., Luo, M., Zhang, Y., Wilkes, D.C., Ge, G., Grieskamp, T., Yamada, C., Liu, T.C., Huang, G., Basson, C.T., et al. (2009). Secreted Frizzled-related protein 2 is a procollagen C proteinase enhancer with a role in fibrosis associated with myocardial infarction. Nat. Cell Biol. *11*, 46–55. https://doi.org/10.1038/ncb1811.

56. Akpulat, U., Onbaşılar, İ., and Kocaefe, Y.Ç. (2016). Tenotomy immobilization as a model to investigate skeletal muscle fibrosis (with emphasis on Secreted frizzled-related protein 2). Physiol. Genom. *48*, 397–408. https://doi.org/10.1152/physiolgenomics.00010.2016.

57. Hinz, B., Phan, S.H., Thannickal, V.J., Prunotto, M., Desmoulière, A., Varga, J., De Wever, O., Mareel, M., and Gabbiani, G. (2012). Recent developments in myofibroblast biology: paradigms for connective tissue remodeling. Am. J. Pathol. *180*, 1340–1355. https://doi.org/10.1016/j.ajpath.2012.02.004.

58. Lu, H., Huang, D., Ransohoff, R.M., and Zhou, L. (2011). Acute skeletal muscle injury: CCL2 expression by both monocytes and injured muscle is required for repair. FASEB J. *25*, 3344–3355. https://doi.org/10.1096/fj.10-178939.

59. Saito, Y., Chikenji, T.S., Matsumura, T., Nakano, M., and Fujimiya, M. (2020). Exercise enhances skeletal muscle regeneration by promoting senescence in fibro-adipogenic progenitors. Nat. Commun. *11*, 889. https://doi.org/10.1038/s41467-020-14734-x.

60. Theret, M., Low, M., Rempel, L., Li, F.F., Tung, L.W., Contreras, O., Chang, C.K., Wu, A., Soliman, H., and Rossi, F.M.V. (2021). In vitro assessment of anti-fibrotic drug activity does not predict in vivo efficacy in murine models of Duchenne muscular dystrophy. Life Sci. *279*, 119482. https://doi.org/10.1016/j.lfs.2021.119482.

61. Todorovic, V., and Rifkin, D.B. (2012). LTBPs, more than just an escort service. J. Cell. Biochem. *113*, 410–418. https://doi.org/10.1002/jcb.23385.

62. Bello, L., Kesari, A., Gordish-Dressman, H., Cnaan, A., Morgenroth, L.P., Punetha, J., Duong, T., Henricson, E.K., Pegoraro, E., McDonald, C.M., et al. (2015). Genetic modifiers of ambulation in the cooperative international neuromuscular research group Duchenne natural history study. Ann. Neurol. *77*, 684–696. https://doi.org/10.1002/ana.24370.

63. Flanigan, K.M., Ceco, E., Lamar, K.M., Kaminoh, Y., Dunn, D.M., Mendell, J.R., King, W.M., Pestronk, A., Florence, J.M., Mathews, K.D., et al. (2013). LTBP4 genotype predicts age of ambulatory loss in Duchenne muscular dystrophy. Ann. Neurol. *73*, 481–488. https://doi.org/10.1002/ana.23819.

64. Heydemann, A., Ceco, E., Lim, J.E., Hadhazy, M., Ryder, P., Moran, J.L., Beier, D.R., Palmer, A.A., and McNally, E.M. (2009). Latent TGF-beta-binding protein 4 modifies muscular dystrophy in mice. J. Clin. Invest. *119*, 3703–3712. https://doi.org/10.1172/JCI39845.

65. van den Bergen, J.C., Hiller, M., Böhringer, S., Vijfhuizen, L., Ginjaar, H.B., Chaouch, A., Bushby, K., Straub, V., Scoto, M., Cirak, S., et al. (2015). Validation of genetic modifiers for Duchenne muscular dystrophy: a multicentre study assessing SPP1 and LTBP4 variants. J. Neurol. Neurosurg. Psychiatry *86*, 1060–1065. https://doi.org/10.1136/jnnp-2014-308409.

66. Morales, M.G., Cabello-Verrugio, C., Santander, C., Cabrera, D., Goldschmeding, R., and Brandan, E. (2011). CTGF/CCN-2 over-expression can directly induce features of skeletal muscle dystrophy. J. Pathol. *225*, 490–501. https://doi.org/10.1002/path.2952.

67. Morales, M.G., Gutierrez, J., Cabello-Verrugio, C., Cabrera, D., Lipson, K.E., Goldschmeding, R., and Brandan, E. (2013). Reducing CTGF/CCN2 slows down mdx muscle dystrophy and improves cell therapy. Hum. Mol. Genet. *22*, 4938–4951. https://doi.org/10.1093/hmg/ddt352.

68. Bassiouni, W., Ali, M.A.M., and Schulz, R. (2021). Multifunctional intracellular matrix metalloproteinases: implications in disease. FEBS J. *288*, 7162–7182. https://doi.org/10.1111/febs.15701.

69. Tatti, O., Vehviläinen, P., Lehti, K., and Keski-Oja, J. (2008). MT1-MMP releases latent TGF-beta1 from endothelial cell extracellular matrix via proteolytic processing of LTBP-1. Exp. Cell Res. *314*, 2501–2514. https://doi.org/10.1016/j.yexcr.2008.05.018.

70. Yu, Q., and Stamenkovic, I. (2000). Cell surface-localized matrix metalloproteinase-9 proteolytically activates TGF-beta and promotes tumor invasion and angiogenesis. Genes Dev. *14*, 163–176.

71. Lin, Y., Wen-Jie, Z., Chang-Qing, L., Sheng-Xiang, A., and Yue, Z. (2020). mir-22-3p/KLF6/MMP14 axis in fibro-adipogenic progenitors

regulates fatty infiltration in muscle degeneration. FASEB J. *34*, 12691–12701. https://doi.org/10.1096/fj.202000506R.

72. Kopinke, D., Roberson, E.C., and Reiter, J.F. (2017). Ciliary hedgehog signaling restricts injury-induced adipogenesis. Cell *170*, 340–351.e12. https://doi.org/10.1016/j.cell.2017.06.035.

73. Holmbeck, K., Bianco, P., Caterina, J., Yamada, S., Kromer, M., Kuznetsov, S.A., Mankani, M., Robey, P.G., Poole, A.R., Pidoux, I., et al. (1999). MT1-MMP-deficient mice develop dwarfism, osteopenia, arthritis, and connective tissue disease due to inadequate collagen turnover. Cell *99*, 81–92. https://doi.org/10.1016/s0092-8674(00)80064-1.

74. Oh, J., Takahashi, R., Adachi, E., Kondo, S., Kuratomi, S., Noma, A., Alexander, D.B., Motoda, H., Okada, A., Seiki, M., et al. (2004). Mutations in two matrix metalloproteinase genes, MMP-2 and MT1-MMP, are synthetic lethal in mice. Oncogene *23*, 5041–5048. https://doi.org/10.1038/sj.onc.1207688.

75. Snyman, C., and Niesler, C.U. (2015). MMP-14 in skeletal muscle repair. J. Muscle Res. Cell Motil. *36*, 215–225. https://doi.org/10.1007/s10974-015-9414-4.

76. Miyazaki, D., Nakamura, A., Fukushima, K., Yoshida, K., Takeda, S., and Ikeda, S.i. (2011). Matrix metalloproteinase-2 ablation in dystrophin-deficient mdx muscles reduces angiogenesis resulting in impaired growth of regenerated muscle fibers. Hum. Mol. Genet. *20*, 1787–1799. https://doi.org/10.1093/hmg/ddr062.

77. Fukushima, K., Nakamura, A., Ueda, H., Yuasa, K., Yoshida, K., Takeda, S., and Ikeda, S.i. (2007). Activation and localization of matrix metalloproteinase-2 and -9 in the skeletal muscle of the muscular dystrophy dog (CXMDJ). BMC Musculoskelet. Disord. *8*, 54. https://doi.org/10.1186/1471-2474-8-54.

78. Nadarajah, V.D., van Putten, M., Chaouch, A., Garrood, P., Straub, V., Lochmüller, H., Ginjaar, H.B., Aartsma-Rus, A.M., van Ommen, G.J.B., den Dunnen, J.T., and 't Hoen, P.A.C. (2011). Serum matrix metalloproteinase-9 (MMP-9) as a biomarker for monitoring disease progression in Duchenne muscular dystrophy (DMD). Neuromuscul. Disord. *21*, 569–578. https://doi.org/10.1016/j.nmd.2011.05.011.

79. Sun, G., Haginoya, K., Chiba, Y., Uematsu, M., Hino-Fukuyo, N., Tanaka, S., Onuma, A., Iinuma, K., and Tsuchiya, S. (2010). Elevated plasma levels of tissue inhibitors of metalloproteinase-1 and their overexpression in muscle in human and mouse muscular dystrophy. J. Neurol. Sci. *297*, 19–28. https://doi.org/10.1016/j.jns.2010.06.031.

80. von Moers, A., Zwirner, A., Reinhold, A., Brückmann, O., van Landeghem, F., Stoltenburg-Didinger, G., Schuppan, D., Herbst, H., and Schuelke, M. (2005). Increased mRNA expression of tissue inhibitors of metalloproteinase-1 and -2 in Duchenne muscular dystrophy. Acta Neuropathol. *109*, 285–293. https://doi.org/10.1007/s00401-004-0941-0.

81. Qi, J.H., Ebrahem, Q., Moore, N., Murphy, G., Claesson-Welsh, L., Bond, M., Baker, A., and Anand-Apte, B. (2003). A novel function for tissue inhibitor of metalloproteinases-3 (TIMP3): inhibition of angiogenesis by blockage of VEGF binding to VEGF receptor-2. Nat. Med. *9*, 407–415. https://doi.org/10.1038/nm846.

82. Fernández, C.A., and Moses, M.A. (2006). Modulation of angiogenesis by tissue inhibitor of metalloproteinase-4. Biochem. Biophys. Res. Commun. *345*, 523–529. https://doi.org/10.1016/j.bbrc.2006.04.083.

83. Wang, X., Sathe, A.A., Smith, G.R., Ruf-Zamojski, F., Nair, V., Lavine, K.J., Xing, C., Sealfon, S.C., and Zhou, L. (2020). Heterogeneous origins and functions of mouse skeletal muscle-resident macrophages. Proc. Natl. Acad. Sci. USA *117*, 20729–20740. https://doi.org/10.1073/pnas.1915950117.

84. Terao, M., Tani, M., Itoi, S., Yoshimura, T., Hamasaki, T., Murota, H., and Katayama, I. (2014). 11beta-hydroxysteroid dehydrogenase 1 specific inhibitor increased dermal collagen content and promotes fibroblast proliferation. PLoS One *9*, e93051. https://doi.org/10.1371/journal.pone.0093051.

85. Zou, X., Ramachandran, P., Kendall, T.J., Pellicoro, A., Dora, E., Aucott, R.L., Manwani, K., Man, T.Y., Chapman, K.E., Henderson, N.C., et al. (2018). 11Beta-hydroxysteroid dehydrogenase-1 deficiency or inhibition enhances hepatic myofibroblast activation in murine liver fibrosis. Hepatology *67*, 2167–2181. https://doi.org/10.1002/hep.29734.

86. Uezumi, A., Ikemoto-Uezumi, M., Zhou, H., Kurosawa, T., Yoshimoto, Y., Nakatani, M., Hitachi, K., Yamaguchi, H., Wakatsuki, S., Araki, T., et al. (2021). Mesenchymal Bmp3b expression maintains skeletal muscle integrity and decreases in age-related sarcopenia. J. Clin. Invest. *131*, e139617. https://doi.org/10.1172/JCI139617.

87. Pawlinski, R., Pedersen, B., Kehrle, B., Aird, W.C., Frank, R.D., Guha, M., and Mackman, N. (2003). Regulation of tissue factor and inflammatory mediators by Egr-1 in a mouse endotoxemia model. Blood *101*, 3940–3947. https://doi.org/10.1182/blood-2002-07-2303.

88. Schonthaler, H.B., Guinea-Viniegra, J., and Wagner, E.F. (2011). Targeting inflammation by modulating the Jun/AP-1 pathway. Ann. Rheum. Dis. *70* (*Suppl 1*), i109–i112. https://doi.org/10.1136/ard.2010.140533.

89. Hafemeister, C., and Satija, R. (2019). Normalization and variance stabilization of single-cell RNA-seq data using regularized negative binomial regression. Genome Biol. *20*, 296. https://doi.org/10.1186/s13059-019-1874-1.

90. Butler, A., Hoffman, P., Smibert, P., Papalexi, E., and Satija, R. (2018). Integrating single-cell transcriptomic data across different conditions, technologies, and species. Nat. Biotechnol. *36*, 411–420. https://doi.org/10.1038/nbt.4096.

91. Satija, R., Farrell, J.A., Gennert, D., Schier, A.F., and Regev, A. (2015). Spatial reconstruction of single-cell gene expression data. Nat. Biotechnol. *33*, 495–502. https://doi.org/10.1038/nbt.3192.

92. Trapnell, C., Cacchiarelli, D., Grimsby, J., Pokharel, P., Li, S., Morse, M., Lennon, N.J., Livak, K.J., Mikkelsen, T.S., and Rinn, J.L. (2014). The dynamics and regulators of cell fate decisions are revealed by pseudotemporal ordering of single cells. Nat. Biotechnol. *32*, 381–386. https://doi.org/10.1038/nbt.2859.

STAR★METHODS

KEY RESOURCES TABLE

REAGENT or RESOURCE	SOURCE	IDENTIFIER
Antibodies		
Rabbit anti- a/b-tubulin	Cell Signaling Technology	Cat# 2148S; RRID: AB_2288042
Rabbit anti-collagen 1a1	Cell Signaling Technology	Cat# 72026S; RRID: AB_2904565
Rabbit anti-fibronectin	Cell Signaling Technology	Cat# 63779S
Rabbit anti-collagen III	Abcam	Cat# ab7778; RRID:AB_306066
IRDye 800CW anti-rabbit IgG	LI-COR Biosciences	Cat# 926-32211; RRID: AB_621843
PerCP-Cy5.5 Rat anti-mouse CD45	BD Biosciences	Cat# 550994; RRID:AB_394003
PE Rat anti-mouse CD45	BD Biosciences	Cat# 553081; RRID:AB_394611
APC Rat anti-mouse CD31	BD Biosciences	Cat# 551262; RRID:AB_398497
PE Rat anti-mouse CD31	BD Biosciences	Cat# 553373; RRID:AB_394819
PE-Cy7 Rat anti-mouse Ly6-A/E (Sca-1)	BD Biosciences	Cat# 558162; RRID:AB_647253
BV421 Rat anti-mouse CD140A (PDGFRa)	BD Biosciences	Cat# 562774; RRID:AB_2728781
PE Rat anti-mouse Integrin α7	R&D Systems	Cat# FAB3518P; RRID:AB_2249296
APC Rat IgG2a, κ Isotype Control	BD Biosciences	Cat# 551139; RRID: AB_10054921
PE Rat IgG2a, κ Isotype Control	BD Biosciences	Cat# 559317; RRID: AB_10050484
PE-Cy7 Rat IgG2a, κ Isotype Control	BD Biosciences	Cat# 552784; RRID: AB_394465
BV421 Rat IgG2a, k Isotype Control	BD Biosciences	Cat# 562602; RRID:AB_11153860
PerCP-Cy5.5 Rat IgG2b, κ Isotype Control	BD Biosciences	Cat# 550764; RRID: AB_393874
PE Rat IgG2b, k Isotype Control	BD Biosciences	Cat# 555848; RRID:AB_396171
Chemicals, peptides, and recombinant proteins		
Mayer's Hematoxylin solution	Millipore Sigma	Cat# MHS16
Eosin Y solution	Millipore Sigma	Cat# HT110116
4% paraformaldehyde solution	Thermo Scientific	Cat# J19943.K2
Poly Mount Xylene	Polysciences	Cat# 24716-120
Collagenase B	Roche Diagnostics	Cat# 11088831001
Dispase II	Roche Diagnostics	Cat# 04942078001
Fetal bovine serum	Corning	Cat# 35-011-CV
Bovine serum albumin	Millipore Sigma	Cat# A7030
Normal mouse serum	Millipore Sigma	Cat# S7273
Lympholyte-M solution	Cedarlane	Cat# CL5035
TRIzol reagent	Invitrogen	Cat# 15596026
RPMI 1640	Gibco	Cat# 11-875-093
RIPA buffer	Pierce Biotechnology	Cat# 89901
cOmplete (protease inhibitor)	Roche Diagnostics	Cat# 04.693.116.001
Bolt 4–12% Bis-Tris mini-gel	Invitrogen	Cat# NW04122
Immobilon PVDF membrane	Millipore	Cat#I SEQ00010
Acridine Orange and Propidium Iodide staining solution	Nexcelom	Cat# CS2-0106
Critical commercial assays		
Vybrant™ DyeCycle™ Violet/SYTOX™ AADvanced™ Kit	Invitrogen	Cat# A35135
EdU Click 647 Kit + EdU	Baseclick GmbH	Cat# BCK647

(*Continued on next page*)

Continued

REAGENT or RESOURCE	SOURCE	IDENTIFIER
Rneasy Micro Kit	Qiagen	Cat# 74004
Super-Script III Reverse Transcriptase Kit	Invitrogen	Cat# 18080051
PowerTrack™ SYBR Green Master Mix	Applied Biosystems	Cat# A46109
BCA protein assay Kit	Pierce Biotechnology	Cat# 23225
Single Cell 3′ Reagents Kits V3.1	10x Genomics	https://assets.ctfassets.net/an68im79xiti/1eX2FPdpeCgnCJtw4fj9Hx/7cb84edaa9eca04b607f9193162994de/CG000204_ChromiumNextGEMSingleCell3_v3.1_Rev_D.pdf
Deposited data		
Single cell-based RNA sequencing data	https://www.ncbi.nlm.nih.gov/geo/	GEO:GSE218201
Experimental models: Organisms/strains		
C57BL/6J mice	The Jackson Laboratory	
mdx^{5cv} mice	The Jackson Laboratory; Chapman VM, et al. PNAS 86(4): 1292–6.	
Oligonucleotides		
Gapdh (Forward): 5′-GTGTTCCTACCCCCAATGTGTC-3′	IDT DNA Oligos	N/A
Gapdh (Reverser): 5′-GTAGCCCAAGATGCCCTTCAGT-3′	IDT DNA Oligos	N/A
Col1a1 (Forward): 5′-GCTCCTCTTAGGGGCCACT-3′	IDT DNA Oligos	N/A
Col1a1 (Reverse): 5′-CCACGTCTCACCATTGGGG-3′	IDT DNA Oligos	N/A
Col3a1 (Forwad): 5′-AACCTGGTTTCTTCTCACCCTTC-3′	IDT DNA Oligos	N/A
Col3a1 (Reverse): 5′-ACTCATAGGACTGACCAAGGTGG-3′	IDT DNA Oligos	N/A
Fn1 (Forward): 5′-AAACTTGCATCTGGAGGCAAACCC-3′	IDT DNA Oligos	N/A
Fn1 (Reverse): 5′-AGCTCTGATCAGCATGGACCACTT-3′	IDT DNA Oligos	N/A
Igf1 (Forward): 5′-CTACAAAAGCAGCCCGCTCT-3′	IDT DNA Oligos	N/A
Igf1 (Reverse): 5′-CTTCTGAGTCTTGGGCATGTCA-3′	IDT DNA Oligos	N/A
Ccn2 (Forward): 5′-AGGACTGCAGCGCGCAATGT-3′	IDT DNA Oligos	N/A
Ccn2 (Reverse): 5′-GAGGCCCTTGTGTGGGTCGC-3′	IDT DNA Oligos	N/A
Mmp2 (Forward): 5′-GCCCCGAGACCGCTATGTCCACT-3′	IDT DNA Oligos	N/A
Mmp2 (Revers): 5′-GCCCCACTTCCGGTCATCATCGTA-3′	IDT DNA Oligos	N/A
Timp1 (Forward): 5′-ACTCGGACCTGGTCATAAGGGC-3′	IDT DNA Oligos	N/A
Timp1 (Reveres): 5′-TTCCGTGGCAGGCAAGCAAAGT-3′	IDT DNA Oligos	N/A
Timp2 (Forward): 5′-GGCAACCCCATCAAGAGGA-3′	IDT DNA Oligos	N/A
Timp2 (Reverse): 5′-CCTTCTGCCTTTCCTGCAATTAG-3′	IDT DNA Oligos	N/A
Mmp14 (Forward): 5′-CTTCAAAGGAGATAAGCACTG-3′	Millipore Sigma	KiCqStart® SYBR® Green Primers: Cat# KSPQ12012
Mmp14 (Reverse): 5′-AGAAGTAGGTCTTCCCATTG-3′	Millipore Sigma	KiCqStart® SYBR® Green Primers: Cat# KSPQ12012
Ltbp4 (Forward): 5′- CCCATTCTTCGAAATATCACC-3′	Millipore Sigma	KiCqStart® SYBR® Green Primers: Cat# KSPQ12012
Ltbp4 (Reverse): 5′- GAAAACCCTCTGAACCATAAG-3′	Millipore Sigma	KiCqStart® SYBR® Green Primers: Cat# KSPQ12012
Lox (Forward): 5′-CACCGTATTAGAAAGAAGCC-3′	Millipore Sigma	KiCqStart® SYBR® Green Primers: Cat# KSPQ12012
Lox (Reverse): 5′-GTCCTTCCTACTTAAGCTAATC-3′	Millipore Sigma	KiCqStart® SYBR® Green Primers: Cat# KSPQ12012
Loxl1 (Forward): 5′-TGCTATGACACATACAATGC-3′	Millipore Sigma	KiCqStart® SYBR® Green Primers: Cat# KSPQ12012
Loxl1 (Reverse): 5′-GAACAATGTACTTGGGGTTC-3′	Millipore Sigma	KiCqStart® SYBR® Green Primers: Cat# KSPQ12012

(*Continued on next page*)

Continued

REAGENT or RESOURCE	SOURCE	IDENTIFIER
Software and algorithms		
GraphPad Prism 8	GraphPad	https://www.graphpad.com/scientific-software/prism/
FlowJo V10	BD Biosciences	https://www.bdbiosciences.com/en-us/products/software/flowjo-v10-software
Image Studio software	LI-COR Biosciences	https://www.licor.com/bio/image-studio/
Image J	NIH	https://imagej.nih.gov/ij/
R package Seurat version 4.0	Satija Lab at NYGC	https://satijalab.org/seurat/
g:Profiler		https://biit.cs.ut.ee/gprofiler/gost
Monocle3		https://cole-trapnell-lab.github.io/monocle3/

RESOURCE AVAILABILITY

Lead contact

Further information and requests for resources and reagents should be directed to and will be fulfilled by the lead contact, Xingyu Wang (wangx20@bu.edu).

Materials availability

This study did not generate unique new reagents or mouse lines.

Data and code availability

Single-cell based RNA sequencing (scRNAseq) data have been deposited to GEO repository (GEO: GSE218201) and are publicly available as of the date of publication. The accession number is also listed in the key resources table. This paper does not report original code. Any additional information required to reanalyze the data reported in this paper is available from the lead contact upon request.

EXPERIMENTAL MODEL AND SUBJECT DETAILS

Animals

C57BL/6J (*WT*) and *mdx*^{5cv} mice (B6 background) were purchased from the Jackson Laboratory (Bar Harbor, ME, USA). Only males were used in this study because DMD only affects males. For scRNAseq analysis, *WT* and *mdx*^{5cv} mice used were at 14 weeks of ages with body weight between 25 and 30 grams. For FACS analysis determining FAP density, an additional time point at 24 weeks of age was used for *mdx*^{5cv} mice with body weight between 30 and 35 grams. Our study protocols were approved by the Institutional Animal Care and Use Committee at the Boston University School of Medicine (Boston, MA, USA.).

METHOD DETAILS

Muscle sample collection

Quadriceps and diaphragm were collected from 14-week-old male *WT* mice, and 14-week-old and 24-week-old male *mdx*^{5cv} mice. Tendons were removed from the tissue specimens. Collected muscle samples were thoroughly washed in 1× phosphate-buffered saline (PBS, pH 7.4) to remove blood contamination.

Histopathological analysis

Collected muscle samples were frozen in liquid nitrogen-chilled isopentane for 30 seconds. Cross sections were then obtained on a Leica cryostat at a thickness of 10 μm. Sections were air-dried for 30 minutes at room temperature and then fixed in 4% (w/v) of paraformaldehyde (Thermo Scientific) for 10 minutes followed by washing in 1× PBS for 5 minutes. Hematoxylin and Eosin (H&E) staining was then performed as following: 1) stained in Mayer's Hematoxylin solution (Millipore Sigma, Burlington, MA, USA.) for 10 minutes, 2) rinsed in warm running tap water for 15 minutes, 3) washed in distilled water for 30 seconds, 4) placed in 95% (v/v) reagent alcohol for 30 seconds, 5) stained in Eosin Y solution (Alcoholic, Millipore Sigma) for 1 minute, 6) dehydrated and cleared through 2 changes each of 95% reagent alcohol, absolute

reagent alcohol, and xylene for 2 minutes each, 7) mounted with Poly Mount Xylene (Polysciences, Warrington, PA, USA). Stained sections were viewed and photographed under a bright-field microscope (Nikon, Y-THR-L).

Muscle single-cell suspension preparation

Single-cell suspension was prepared by collagenase/dispase digestion.[83] Quadriceps and diaphragm samples (less than 250 mg) were minced in 2.5 mL digestion solution (1 U/ml collagenase B and 1 U/ml dispase II (Roche Diagnostics, Indianapolis, IN, USA) in 1× PBS) and incubated at 37°C for 1 hour. The reaction was terminated by adding 10 mL PBS containing 10% (v/v) fetal bovine serum (FBS, Corning, Glendale, AZ, USA). The mixture was then filtered through a 70-μm cell strainer and centrifuged at 250 g for 5 minutes. The pellet was collected, and the supernatant was centrifuged again at 250 g for 5 minutes at 4°C. The pellet was combined with the pellet from the first centrifugation, washed with PBS, and centrifuged at 670 g for 10 minutes at 4°C. The pellet was re-suspended in 3 mL PBS and filtered through a 40-μm cell strainer. Cell suspension was layered on equal volume of the Lympholyte-M solution (Cedarlane, Burlington, NC, USA) and centrifuged at 2,100 g for 45 minutes at room temperature. Cells at the interface were collected in 10 mL PBS containing 10% FBS, pelleted by centrifugation at 670 g for 10 minutes at 4°C, and re-suspended in appropriated buffer for following analysis.

Flow cytometry analysis and cell sorting

Single-cell pellets were washed once in ice-cold FACS buffer (1× PBS, 0.5% (w/v) bovine serum albumin (BSA, Millipore Sigma), 0.1% (w/v) sodium azide), centrifuged at 500 g for 3 minutes at 4°C, and re-suspended in ice-cold FACS staining buffer (1× PBS, 2% (w/v) BSA, 2% (v/v) normal mouse serum (Millipore Sigma).

For FACS analysis of different cell types, cells were stained on ice for 20 minutes with fluorescence-labelled antibodies targeting cell-type specific markers: Fibro/Adipogenic progenitors (FAPs) were identified as Sca-1^{+}PDGFRα^{+}CD45^{-}CD31$^{-}\alpha$7-integrin^{-} cells, endothelial cells (ECs) were identified as CD31^{+}CD45^{-} cells, and muscle satellite cells (MuSCs) were identified as α7-integrin^{+}CD45^{-}CD31^{-}Sca-1^{-} cells. Fluorescence-labelled corresponding normal IgG isotypes were included as negative controls for gating. All antibodies were from commercial providers (See key resources table for details) and diluted for staining following manufacturer's recommendations. After staining, cells were washed twice with FACS buffer and analyzed on a LSR II (BD Bioscience, San Jose, CA, USA) with BD FACSDiva™ software. Collected data were then analyzed using FlowJo software (Tree Star, Inc., Ashland, OR, USA).

To clean up single cell suspension for subsequent single-cell based analysis, cell sorting based on FSC/SSC was performed to exclude dead cells, cell duplexes, and tissue debris. Sorting FAPs and non-FAPs for qRT-PCR analysis were performed with antibodies listed above. Cell sorting was done by the Flow Cytometry Core of Boston University School of Medicine. Collected cells from 5 individual male mice were combined, and pelleted by centrifuging at 300 g for 10 minutes. For scRNAseq analysis, pellets were re-suspended in FBS supplemented with 10% of DMSO, and cryopreserved in liquid nitrogen. For qRT-PCR analysis, pellets were dissolved in TRIzol reagent (Invitrogen, Waltham, MA, USA) for RNA preparation.

FAP apoptosis assay

Muscle single-cell suspension was first stained with antibodies identifying FAPs as described in the section of flow cytometry analysis and cell sorting. After being washed twice with FACS buffer, cells were again re-suspended in FACS buffer and stained with Vybrant™ DyeCycle™ Violet/SYTOX™ AADvanced™ reagents (Invitrogen) following manufacturer's instruction. Stained cells were analyzed by flow cytometry immediately. Apoptotic FAPs were identified as Vybrant^{+}SYTOX^{-}.

FAP proliferation assay

Mdx^{5cv} mice at 14 weeks of age received intraperitoneal injection of EdU (100 mg/mouse, Baseclick GmbH, Germany). Quadriceps and diaphragm were then collected 24 hours later and single-cell suspension was prepared as described in the section of muscle single-cell suspension preparation. FAP proliferation was then analyzed by determining the incorporation of EdU using EdU Click 647 Kit (Baseclick GmbH, Germany) following manufacturer's instruction, combined with FACS staining and analysis of FAPs as described in the section of flow cytometry analysis and cell sorting.

RNA preparation and qRT-PCR

Total RNA samples were prepared using TRIzol reagent (Invitrogen). Samples of FAPs and non-FAPs were prepared by cell sorting as stated above and dissolved in TRIzol reagent. To prepare whole-muscle RNA, quadriceps and diaphragm, collected from 14-week-old male *WT* and *mdx*^{5cv} mice, were homogenized in TRIzol reagent using Bead Mill 24 homogenizer (Fisher Scientific). Total RNA was then prepared following manufacturer's instruction. TRIzol-prepared total RNA was further cleaned up using RNeasy Micro Kit (Qiagen, Germantown, MD, USA) following manufacturer's instruction. Concentration of cleaned RNA was measured using NanoDrop 2000 Spectrophotometer (Thermo Scientific). 1 μg of total RNA was then reverse-transcribed into cDNA using Super-Script III Reverse Transcriptase system (Invitrogen) following manufacturer's instruction. Expression of genes at mRNA level was then analyzed by real-time PCR with PowerTrack™ SYBR Green Master Mix (Applied Biosystems, Waltham, MA, USA) using StepOne™ Real Time PCR System (Applied Biosystems). Sequences and providers of the primers used are listed in key resources table. The sequences and target genes of the primers were listed in key resources table. Data was calculated by ΔΔCt method. For sorted cell analysis, data was presented as bar graph with error bar showing standard deviation of triplicated PCR results. For whole muscle analysis, data were presented as scatter plot showing results of each individual samples.

Western blot

Quadriceps and diaphragm, collected from 14-week-old male *WT* and *mdx*^{5cv} mice, were homogenized in RIPA buffer (Pierce Biotechnology, Waltham, MA, USA) supplemented with cOmplete protease inhibitor cocktail (Roche Diagnostic). After centrifugation (10,000 ×g for 15 minutes), the protein concentration was quantitated by Pierce BCA protein assay kit (Pierce Biotechnology). 50 μg of protein lysate were run on 4–12% Bis-Tris mini-gel (Invitrogen) under reducing condition then transferred to PVDF membranes (Immobilon). Blots were blocked with 5% (w/v) of non-fat milk in TBS-T (1× Tris-buffered saline (pH7.6) with 0.1% (v/v) Tween 20) and then incubated with primary antibodies include α/β-tubulin (1:1000 dilution), collagen 1α1 (1:500), fibronectin (1:250) (all purchased from Cell Signaling Technology, Danvers, MA, USA), and collagen III (1:500) (Abcam, Waltham, MA, USA). Signals were detected by IRDye 800 or 680 (LI-COR Biosciences, Lincoln, NE)-conjugated secondary antibodies with appropriate species specificity. Immunoblots were visualized by the Image Studio software (LI-COR Biosciences) that accompanies the LI-COR Odyssey infrared system (LI-COR Biosciences).

Single-cell cDNA library preparation and sequencing

Cryopreserved cells were thawed in a 37°C water bath for two minutes. The thawed content was added dropwise into 9 mL of warm freshly prepared RPMI 1640 (Gibco) with 20% of FBS, spun 300 g for 5 minutes, and re-suspended in 5 mL of RPMI with10% of FBS. The cells were counted, and viability was assessed using Acridine Orange and Propidium Iodide staining followed by counting on a K2 Cellometer (Nexcelome, Lawrence, MA, USA). Next, scRNAseq was performed following the Single Cell 3′ Reagents Kits V3.1 User Guidelines (10x Genomics, Pleasanton, CA, USA). All samples were above 70% viability. Cells were loaded to target 5,000 cells final for generating the single-cell emulsion (Chromium Single Cell 3′ Chip kit A v2 PN-12036 or v3 chip kit B PN-2000060). Reverse-transcription (RT) was performed in the emulsion, cDNA amplified, and library constructed with v3.1 chemistry. Libraries were indexed for multiplexing (Chromium i7 Multiplex kit PN-12062). Following preparation, libraries were quantified by Qubit 3 fluorometer (Invitrogen) and quality was assessed by Bioanalyzer (Agilent Technologies, Santa Clara, CA, USA). Equivalent molar concentrations of libraries were pooled, and the reads were adjusted after sequencing the pools in a Miseq (Illumina, San Diego, CA, USA). The libraries were then sequenced in a Novaseq 6000 (Illumina) at the New York Genome Center (NYGC, New York, NY, USA) following 10× Genomics recommendations.

Single cell-based mRNA sequencing analysis

The gene × cell expression matrices were loaded to the R package Seurat version 4.0 (https://cran.r-project.org/web/packages/Seurat/index.html) for downstream analyses.[31] Cells of low quality, defined by the detectable expression of fewer than 200 genes per 1000 Unique Molecular Identifiers (UMI) and the presence of more than 7.5% mitochondria content, were filtered out.[31] The Seurat default global-scaling normalization method LogNormalize was used to normalize the feature expression measurements for each cell by the total expression, multiplies this by a scale factor and log-transforms the result. The

Seurat default global-scaling normalization method, "LogNormalize", was used for scaling the data.[89] The method Vst was used to identify highly variable features in function FindVariableFeatures.

A shared-nearest neighbor (SNN) graph–based clustering method was constructed to identify discrete cell populations. Then the obtained clusters were optimized by using the "FindClusters" function.

Linear dimensional reduction PCA was performed on variable genes. A clear Elbow in the plot of the PC standard deviation was used to define the significant PCs. Based on the identified PCs above, non-linear dimensional reduction technique UMAP was performed.[89–91] Differentially Expressed Genes (DEGs) were calculated and obtained by the function of FindAllMarkers based on the Wilcoxon rank sum test.[31] Top marker genes in each cluster shown in Heatmap were ordered by log fold-change of the average expression. Differential gene expression analysis was performed in each of the cell clusters, and the log transformed fold changes (log_2FC) were used to perform hierarchical clustering between genes.

Functional enrichment analysis

We used g:Profiler webserver (https://biit.cs.ut.ee/gprofiler/gost) to perform functional enrichment analysis for the identified DEGs in individual clusters or subclusters. Top DEGs (adj. p-value < 0.05) were tested for enrichment of biological pathways with Gene Ontology (GO), Reactome, CORUM and KEGG. Results from different databases were compared to ensure the reliability of the analysis.

Pseudotime trajectory analysis

The cells of FAP clusters were further analyzed using Monocle for pseudotime trajectory.[92] Seurat objects were converted to CellDataSet objects using the as.cell_data_set function from SeuratWrappers. The trajectories were built using Monocle 3 (https://cole-trapnell-lab.github.io/monocle3/docs/citations/, https://satijalab.org/signac/articles/monocle.html). Each sample was analyzed separately by the same procedure. Interactive function order cells was used to select cells as the root nodes in the graph. The function get_earliest_principal_node was applied to identify the root principal points.

Venn diagram

Differential gene expression among FAPs of 4 muscles (WT diaphragm, *mdx*^{5cv} diaphragm, WT quadriceps, and *mdx*^{5cv} quadriceps) were determined by Seurat FindMarkers function, using a log fold-change threshold of 0.5 and an adjusted p value cutoff of 0.05. Venn diagram was prepared using Venny2.1.

QUANTIFICATION AND STATISTICAL ANALYSIS

Data were analyzed using GraphPad Prism 8 software (GraphPad Software, San Diego, CA, USA). The Mann-Whitney test was performed to compare between two groups; the Kruskal-Wallis test followed by Dunn's test was performed to compare multiple (>=3) groups. A p value of <0.05 was considered statistically significant.